Main Manuscript for

A Cell-Permeable Fluorescent Probe Reveals Temporally Diverse PI(4,5)P2 Dynamics Evoked by Distinct GPCR Agonists in Neurons

Rajasree Kundu[†1], Samsuzzoha Mondal[†1], Akshay Kapadia[†1], Antara A. Banerjee[†2], Oleksandr A. Kucherak[3], Andrey S. Klymchenko[3], Sandhya P. Koushika[2], Ravindra Venkatramani[1], Vidita A. Vaidya[2], Ankona Datta[1*]

[1]Department of Chemical Sciences, Tata Institute of Fundamental Research, 1 Homi Bhabha Road, Mumbai-400005, India.

[2]Department of Biological Sciences, Tata Institute of Fundamental Research, 1 Homi Bhabha Road, Mumbai-400005, India.

[3] Laboratoire de Bioimagerie et Pathologies, UMR 7021 CNRS, Faculté de Pharmacie, Université de Strasbourg, Strasbourg, CS 60024, France.

*Corresponding author: ankona@tifr.res.in

[†]equally contributed

Author Contributions: AD guided, designed, conceptualized, and oversaw the project; RK and SM performed the simulations, designed and developed probes, conducted in vitro experiments, and analyzed the data; AK and AAB conducted experiments in cells and primary cortical neurons and analyzed data; SPK assisted in planning and setting up *C.elegans* experiments and SM performed the experiments; VAV assisted in setting up and planning neuronal experiments; RV assisted in molecular dynamics simulations and analysis; OAK and ASK synthesized and shared polarity-sensitive dye; RK, SM, AK, AAB, VAV, and AD wrote the paper. All authors reviewed the results and the manuscript and approved the final version of the manuscript.

Competing Interest Statement: The authors declare no competing interest.

Keywords

Lipid dynamics;

PI(4,5)P2 sensor;

Gq-coupled receptor;

Live Imaging;

Imaging PI(4,5)P2 Dynamics;

Serotonergic Psychedelic;

5-HT

Abstract

Lipids, key structural constituents of cell membranes, are amongst the first responders to cell signals.[1] Bystander lipid molecules are also critical components of a signaling response when a chemical stimulus is received at a cell-surface receptor.[2,3] At the crux of the spatiotemporal dynamics of lipid signaling response are phosphoinositides.[4,5] Indeed, phosphoinositides like phosphatidylinositol-(4,5)-bisphosphate (PI(4,5)P2), present in the inner-leaflet of eukaryotic cell membranes, form the link between signal reception at a G-protein coupled receptor (GPCR) and downstream signal transmission.[6] The role of signaling lipids in driving the heterogeneity of signaling responses that ensue upon the binding of distinct ligands to the same GPCR remains unclear, and is central to understanding divergent physiological outcomes of ligand-binding. Different ligands/agonists upon binding to the same GPCR can invoke contrasting behavioral effects. Key examples are the divergent signaling signatures evoked by hallucinogenic versus non-hallucinogenic agonists at the serotonin2A (5-HT_{2A}) receptor.[7] We asked whether probing PI(4,5)P2 dynamics could uncover the earliest of differences in signaling that arise upon distinct ligands binding to the 5-HT_{2A} receptor. The challenge was to track rapid < 1 min PI(4,5)P2 dynamics in living systems.[8] Here we report a computationally-designed, rapid-response, reversible, photo-stable, fluorescent probe that permeates living cells, neurons, and a multicellular organism within few min of direct incubation and distinctly visualizes PI(4,5)P2 pools, in an optical imaging setup. This novel probe facilitates rapid tracking of seconds to sub-minute PI(4,5)P2 dynamics that arise from ligand-binding at the serotonergic receptor. Our results reveal that a hallucinogenic ligand at the 5-HT_{2A} receptor leads to a slower rate of PI(4,5)P2 depletion when compared to a non-hallucinogenic ligand, but has a sustained longer effect. The ability of our designer chemical probe in timing early seconds-minute timescale lipid dynamics in living cells opens avenues for tracking early time-point molecular events in neuronal response to chemical and physical stimuli.

Main Text

The plasma membrane is far more than a mere structural boundary, it is the interface where signal transduction commences, a gateway for all cellular communication, and an active signaling platform.[1] Central to the roles of the plasma membrane in cellular processes are phospholipids (PLs) that make the membrane.[9] The localization/distribution/level of a phospholipid in a cell membrane is highly dynamic and changes temporally in seconds to minutes.[5,10] Tracking this dynamic change in phospholipid distribution and levels in a cell membrane, live, is necessary to understand how the membrane regulates and times cellular signals, transport, and communication.

In the playground of lipid-mediated signal transmission and cellular regulation, phosphoinositides are singularly important.[4-6,11] Phosphoinositides are almost exclusively present in the inner leaflet of cell membranes toward the cytoplasmic interface, and in organelle membranes.[5] The levels of phosphoinositides in cell membranes are ~1-5% of the total phospholipid content of the membrane.[5,12] While low in abundance, these lipids are functionally critical and not only mediate classical signal transduction like neurotransmission via G protein-coupled receptors (GPCRs),[6] but also regulate ion channels,[13] and impinge on key cellular processes such as exocytosis and endocytosis.[4,5] Recent studies reveal that both the composition and localization of specific phosphoinositide in proximity to membrane proteins such as GPCRs can influence their activity.[2] Hence, by visualizing phosphoinositide dynamics within cell membranes we can gain a direct handle into elucidating the link between lipid dynamics and cellular signaling processes. We asked if ligands at the same GPCR, that ultimately have divergent behavioral effects, show phosphoinositide-mediated signaling differences as early as few seconds into signal initiation.

A major challenge that we needed to overcome in order to address this question was the ability to visualize the seconds-minute dynamics of signal-mediating phosphoinositides within living cells and neurons. Why is that so? The current gold-standard in phosphoinositide imaging relies heavily on non-responsive protein-based fluorescent sensors (**Table-S1**).[14] These large probes are diffusion-limited[15] and especially in the crowded intracellular environment often cannot catch subtle differences in lipid dynamics in seconds-minute timescale,[10,16] specifically, apparently small but functionally significant effects related to neurotransmission. An example is the differences in early time point signaling events that occur when distinct ligands bind the same cell-membrane receptor.[7] Apart from their large size, these probes, based on protein-domains that bind to phospholipids, often cannot distinguish between phospholipids and their soluble headgroup counterparts which are second messengers. Fluorescently tagged artificial phosphoinositides are an alternative to protein-based sensors.[17-19] However, modified lipids can be mis-localized in the cell membrane due to their altered chemical properties compared to native lipids.[8,11,18] Importantly, their in-cell dynamics is different from native counterparts.[8] Here, we report that a rapid response, reversible, ratiometric, cell-permeable short (12 amino acid) peptide-based, photo-stable, fluorescent phosphoinositide probe, times the early seconds-minute

differences in signaling events at the cell membrane of neurons in response to the binding of a hallucinogenic versus a non-hallucinogenic agonist of the serotonin$_{2A}$ (5-HT$_{2A}$) receptor. These results open avenues to access the earliest of events in lipid-mediated signaling that can in turn drive differential signaling outcomes, using cell-permeable lipid responsive chemical tools.

Designing a short-peptide based, ratiometric, rapid-response, cell-permeable, fluorescent probe for phosphatidylinositol-(4,5)-bisphosphate

First, we set-forth to design and develop a low-molecular weight (1-3 kDa), cell-permeable, rapid-response, photo-stable, fluorescent probe for phosphatidylinositol-(4,5)-bisphosphate (PI(4,5)P2). PI(4,5)P2 (**Extended Data Fig. 1**) regulates classical signal transduction. When a GPCR binds to a chemical ligand like a neurotransmitter or an agonist, the enzyme phospholipase C (PLC) cleaves the headgroup of PI(4,5)P2, to release inositol-1,4,5-trisphosphate (IP3) which then acts as a second messenger in signaling pathways (**Extended Data Fig. 10**).[20] PI(4,5)P2 is almost exclusively present in the inner leaflet of the plasma membrane. Since, we wanted to track and time initial PI(4,5)P2-mediated signaling events during ligand/agonist-receptor interaction at the cell-membrane, we needed a cell-permeable probe that would selectively and sensitively respond to PI(4,5)P2 over other cellular PLs.

A powerful approach in the design of probes is to use polarity-sensitive dyes, which change their emission color in response to local microenvironment variations produced by bio-molecular interactions.[21] In our previous work we had developed peptide-based fluorescent, ratiometric probes for phosphoinositides which responded to both PI(4,5)P2 and phosphatidylinositol-4-phosphate (PI(4)P) (**Extended Data Fig. 1**) without any specificity toward a specific phosphoinositide.[22] The probe design involved attaching a polarity sensitive dansyl dye to a phosphoinositide binding peptide segment of the actin-regulatory protein Gelsolin (Gel 150-169). These phosphoinositide probes had low photo-stability which precluded applications in imaging live cell dynamics over several min. Therefore, key features that we desired in a PI(4,5)P2 probe that would track live PI(4,5)P2 dynamics were, selectivity, rapid cell-permeability in min timescale for easy applicability, sensitivity toward lower ~ 1 mol% PI(4,5)P2, reversible response to visualize dynamics, and importantly photo-stability for time-lapse imaging over several minutes. Our strategy for imaging PI(4,5)P2 dynamics was to design a probe with a cell-permeable peptide-binding unit that would bind to PI(4,5)P2 and provide a specific conformational change that could be leveraged to sense the lipid selectively. The work-flow that we devised to attain a PI(4,5)P2 selective probe involved molecular dynamics simulations on Gel 150-169 (Gel-20aa) and Gel 158-169 (Gel-12aa) peptides in the presence of different phosphoinositide headgroups. The driver for the selection of these peptides was their proven ability to bind to phosphoinositides even when removed from

the parent protein.[22] We asked if there were any specific differences in the interaction of the peptides with different phosphoinositides, that could be leveraged to generate a PI(4,5)P2 selective probe.

All atom molecular dynamics (MD) simulations were performed on both the Gel-20aa and Gel-12aa peptides on a phospholipid bilayer (**Extended Table 1**). The Gel-20aa peptide was reported to adopt a helical conformation in the presence of PI(4,5)P2, hence, an NMR structure of the helical form (PDB ID: 1SOL)[23] of the peptide was used as a model for the simulations. The structure of the shorter Gel-12aa sequence was modeled based on the structure of Gel-20aa by deleting the eight C-terminal amino acids from the Gel-20aa sequence *in silico*. Three 100 Å x 100 Å membrane bilayers made of phosphatidylcholine (PC) molecules were created where a single phosphoinositide molecule, either PI(4)P or PI(4,5)P2 or phosphatidylinositol-3,4,5-trisphosphate, (PI(3,4,5)P3) (**Extended Data Fig. 1**), was inserted into one leaflet of the PC membrane to afford 0.74 mol% of PI(4,5)P2 on a single leaflet of the bilayer (**Fig. 1a-c**). This value was within the expected range of the biological abundance (0.5-1 mol%) reported for PI(4,5)P2 and PI(4)P.[12,24] PI(3,4,5)P3 while at least 100 fold lower in abundance than PI(4,5)P2 and PI(4)P, was included in the calculations as a control because of its high-structural similarity to PI(4,5)P2. In our simulations, the positively charged residues in the C-terminus of Gel-20aa were seen to form electrostatic contacts with the negatively charged phosphate moieties of the phosphoinositide headgroups (**Fig. 1a-c, Video-1**). The binding modes of the peptide C-terminus with each of the three phosphoinositides were different. For example, R20 and K17 formed electrostatic contacts with PI(4,5)P2 throughout the entire course of the simulations (**Fig. 1b, Video-1)**, while R20 and R19 formed electrostatic contacts with PI(3,4,5)P3 (**Fig. 1c, Video-1**). We estimated average non-bonding interaction energies ($\boldsymbol{\Delta E_{NB}}$) between positively charged residues of the peptide lying within 3 Å of a phosphoinositide headgroup, and the phosphoinositide headgroup. The peptide showed the highest $\boldsymbol{\Delta E_{NB}}$ toward PI(3,4,5)P3 followed by PI(4,5)P2 and PI(4)P (**Fig. 1d, Extended Data Fig. 4b, Extended Table 2**). Over the course of the 200 ns simulations, within the first ~13 ns, the peptide aligned parallelly to the membrane allowing other residues as well as the N-terminus to interact with the membrane (**Video-1**). The N-terminus of the peptide dipped into the membrane multiple times when PI(4,5)P2 was present, within the first 30 ns of the simulation (**Extended Data Fig. 4a**). The reproducibility of the event was confirmed by running additional short 30 ns simulations (**Extended Data Fig. 4a**). We noted that the N-terminus inserted itself deeper into the membrane for PI(4,5)P2 simulations when compared to that of PI(4)P and PI(3,4,5)P3 (**Fig. 1e, Extended Table 2**). The percentage helicity for the Gel-20aa peptide was the lowest for the simulation performed in the presence of PI(4,5)P2 (**Fig. 1f**), throughout the course of the simulation.

Based on these results we concluded that the N-terminus of the Gel-20aa peptide afforded differential interaction with the membrane in the presence of different phosphoinositides. A closer inspection of the structures of the peptide on membranes with the three different phosphoinositides, hinted that whenever the residue K17 formed an electrostatic contact with the headgroup, the helicity of the peptide was lower (**Video-**

1, Fig. 1f). Specifically, in the case of interaction of the peptide with PI(3,4,5)P3 where K17 did not make any contact with the headgroup throughout the course of the 200 ns simulation, the percentage helicity was higher than the other phosphoinositides (**Video-1, Fig. 1f**). The conformational flexibility arising from the opening of the helix when K17 interacted with the headgroup might lead to increased membrane dipping of the Gel-20aa N-terminus observed for PI(4,5)P2.

The interaction of the shorter peptide, Gel-12aa, with different phosphoinositide headgroups (**Extended Data Fig. 3a-c**) was similar to that of Gel-20aa (**Video-2**). This was not unexpected because the C-terminus of both the peptides was identical. The non-bonding energies of the Gel-12aa peptide toward different phosphoinositide headgroups followed a similar trend as Gel-20aa (**Extended Data Fig. 3d-f)**, except that the ΔE_{NB} values of the peptide interacting with PI(3,4,5)P3 and PI(4,5)P2 were now closer, **(Extended Data Fig. 4c, Extended Table 2**). We noted that despite the differences in N-terminus residues of both peptides, the N-terminus dipping feature was retained over the course of all simulations for the shorter peptide (**Video-2, Extended Data Fig. 3g-i**) with the maximum dipping observed for PI(4,5)P2 (**Extended Table 2**). The short peptide was not helical, based on the simulations, and hence the differential N-terminal dipping observed for the shorter peptide may be attributed to differences in the electrostatic interactions between the cationic amino acids at the C-terminus and phosphoinositide headgroups.

Taken together, the MD simulations for both the Gel-20aa and the Gel-12aa peptides indicated that the extent of dipping of the N-terminus into the membrane was different for the three phosphoinositides studied. We decided to use this feature to develop PI(4,5)P2 selective fluorescent probes. Since the simulations predicted that the N-terminus of the peptides afforded maximum dipping upon interaction with PI(4,5)P2, our strategy was to attach a polarity sensitive dye to the N-terminus of both peptides with the expectation that the resultant N-terminal dye-conjugated peptides might act as PI(4,5)P2 probes (**Fig. 1g**). Next, we needed to select a photo-stable polarity sensitive dye with a significant two-photon absorption cross-section. Photo-stability would allow quantitative imaging of live lipid dynamics and multi-photon excitation at near-infrared[25] would improve depth penetrability in tissue samples and the detection sensitivity due to minimal background from autofluorescence. The dye that we zeroed in on was a methyl substituted fluorene dye MFR. Previously, a push-pull fluorene dye FR_0 was reported,[26] which exhibited superior two-photon cross-section (σ_2 400 GM), sensitivity to polarity, and photo-stability (τ_p 360 min in ethanol), compared to popular prodan- and dansyl-based polarity-sensitive dyes.[21] Here, we applied its dimethylamino-analogue MFR,

bearing a carboxylate group, for developing our probes. Two probes, MFR-VVQRLFQVKGRR (**MFR-12aa**) and MFR-KHVVPNEVVVQRLFQVKGRR (**MFR-20aa**) were therefore designed as depicted in **Extended Data Fig. 2**.

MFR-20aa and MFR-12aa are PI(4,5)P2 selective and sensitive probes

MFR-20aa and **MFR-12aa** were synthesized via a solid-phase synthetic strategy and purified (**Fig S1, S2**). In order to test whether the probes afforded a selective response toward a specific phosphoinositide over other physiologically relevant phospholipids, small unilamellar vesicles (SUVs) of ~ 100 nm diameter were used as model membranes. SUVs containing 5% phosphoinositide in phosphatidylcholine (PC), the major phospholipid component of eukaryotic cell membranes, were prepared and characterized. SUVs containing 20% of several physiologically more abundant phospholipids including phosphatidylserine (PS), phosphatidylinositol (PI), phosphatidylglycerol (PG), and phosphatidylethanolamine (PE) in PC were also included in the experiments. 100% PC SUVs served as control. Since both the probes were completely water-soluble, all in vitro experiments described henceforth were performed in aqueous buffer.

Upon titrating with 5% PI(4,5)P2 in PC SUVs, a 90 nm blue shift (λ_{max} shifted from 575 nm to 485 nm, λ_{ex} 390 nm) was observed for **MFR-20aa** (**Extended Data Fig. 5a**). Concomitantly, a 70 times enhancement was observed for the emission intensity at 480 nm, at saturating lipid concentration. Similarly, **MFR-12aa** afforded a 70 nm spectral shift (λ_{max} shifted from 580 nm to 510 nm, λ_{ex} 390 nm) and 100 times fluorescence enhancement at 480 nm, at saturating lipid concentration (**Fig. 1h**). Hence, **MFR-20aa** and **MFR-12aa** provided dual ratiometric and 'turn-on' emission response toward PI(4,5)P2. Further, this spectral response suggests that after the peptide binds to PI(4,5)P2, the MFR dye is transferred from polar aqueous environment to the low-polar environment of the lipid membrane as predicted from the computational studies.

The in vitro fluorescence titration data was fitted to a 1:1 probe: lipid binding model (Methods Section 5) to obtain association constant (K_a) values for each probe toward all tested physiologically relevant phospholipids. Both probes showed the highest association constants toward PI(4,5)P2. Importantly, the binding toward PI(4)P was significantly lower for both probes when compared to PI(4,5)P2, as predicted by the computational analysis of the MD simulations. **MFR-12aa** and **MFR-20aa** afforded at least 20 times higher affinity toward PI(4,5)P2 over phosphatidylserine (PS) which is the major anionic PL (10-15%) present on the inner leaflet of the eukaryotic plasma membrane (**Fig. 1i** and **Extended Data Fig. 5b**). Both probes afforded a ~ 1.7-1.8 times higher affinity toward PI(4,5)P2 over PI(3,4,5)P3. Since PI(3,4,5)P3 is present in low nM levels in resting cells while PI(4,5)P2 is present in µM levels we concluded, that the MFR-labelled peptides could act as selective and sensitive PI(4,5)P2 probes in cellulo. The limit-of-detection (LOD) of **MFR-12aa** toward PI(4,5)P2 was obtained from the in vitro 'turn-on' response as 220 nM while that for **MFR-20aa** was obtained as 350 nM. From these results we concluded that the shorter peptide-based probe **MFR-12aa** had a similar

selectivity, but higher sensitivity as compared to the longer peptide-based probe **MFR-20aa** and hence would be apt for detection of physiological PI(4,5)P2 levels and dynamics. Further, the response of **MFR-12aa** toward PI(4,5)P2 remained unaffected in the presence of the soluble second messenger IP3 (**Extended Data Fig. 6)**. This was an advantage over protein-based sensors which often bind to both PI(4,5)P2 and IP3 leading to low specificity toward PI(4,5)P2. Because the shorter size of the **MFR-12aa** probe could lead to enhanced cell-permeability, we decided to take it forward to test its applicability toward imaging PI(4,5)P2 dynamics in the specific context of agonist-induced GPCR signaling.

Before proceeding to in cell evaluation of **MFR-12aa**, we further tested the sensitivity of the probe toward detection and imaging of low ~ 1-2 mol% PI(4,5)P2 in model membranes in a confocal fluorescence microscopy setup. Giant unilamellar vesicles (GUVs) with diameter 20-30 µm were prepared with 0-5 mol% of PI(4,5)P2 in PS (20 mol%) and PC (80-75 mol%). PS was used as a component of the GUVs since it is the most abundant anionic PL in eukaryotic cell membranes.[27] GUV images were recorded via two-photon excitation at 780 nm. Emission was collected in both the blue channel, 480-520 nm, which represented the emission from mainly the PI(4,5)P2 bound probe and the orange channel, 580-620 nm, which represented emission from both PI(4,5)P2 bound and unbound probe. The **MFR-12aa** probe clearly lighted up GUVs with 1 mol% PI(4,5)P2 and showed a progressive increase in blue/bound channel emission intensity as the mol% of PI(4,5)P2 was increased in the vesicles (**Fig. 1j, k**). Importantly, control GUVs containing no PI(4,5)P2 but only 20% PS in PC did not afford any emission in the blue channel demonstrating the distinct selectivity of **MFR-12aa** toward PI(4,5)P2 (**Fig. 1j**). This result indicated that the probe had the potential to detect PI(4,5)P2 in the cellular milieu that would have a similar membrane composition.

MFR-12aa images PI(4,5)P2 pools in live cells and in a multi-cellular organism

We next tested whether **MFR-12aa** could permeate cell membranes and image PI(4,5)P2 in living cells. The probe entered living cells within 5-15 min of direct incubation (**Fig 1l, Extended Data Fig. 7 and Fig. 4a-d)**. Importantly, the probe could enter both cultured mammalian cells like HEK293T and primary cortical neurons (**Fig 1l, Extended Data Fig. 7 and Fig. 4a-d)**. The probe did not affect cell-viability up to a tested concentration of 10 µM in HEK293T cells (**Extended Data Fig. 8**) and because of its apt sensitivity could be employed at as low as 1 µM incubation levels for imaging experiments in living cells. When HEK293T cells incubated with the **MFR-12aa** probe were imaged under a fluorescence confocal microscopy setup, fluorescence emission was observed from the cytoplasmic regions of the cell, in the orange channel (580-620 nm) which represents emission from both the free and PI(4,5)P2 bound probe (**Extended Data Fig. 7)**. This data showed that the probe was cell-permeable. The blue channel emission (480-520 nm) which represents emission from

predominantly the PI(4,5)P2 bound probe was observed from the plasma membrane implying that the probe could image plasma membrane PI(4,5)P2 pools.

We next proceeded to explore the ability of the probe to image PI(4,5)P2 pools in vivo, in a multicellular organism. We chose *C.elegans* as a model organism since these are optically transparent microscopic organisms and have a well-defined nervous system. Transgenic *C.elegans* (*gqIs25*) that overexpress PI(4)P-5-kinase (PI5K) in neuronal cells were specifically used for the experiments. The enzyme PI5K converts PI(4)P to PI(4,5)P2 and previous quantification of PI(4,5)P2 levels in the neurons of *gqIs25* showed ~ 40% higher PI(4,5)P2 levels when compared to the neurons of wild-type *C.elegans* (*N2*) strains.[28] Hence, this multicellular model system provided a unique handle to not only test the in vivo applicability but also importantly validate the PI(4,5)P2 selectivity of the probe.

Live *C.elegans* were directly incubated with the probe in aqueous buffer and anesthetized prior to confocal imaging. Confocal images of the live worms showed bright fluorescence in orange (**Extended Data Fig. 9**) and blue emission channels (**Fig. 2c, d**), from the mouth along with emission from the pharynx, and regions surrounding these organs for both the wild-type *N2* strain and the transgenic *gqIs25* strain (**Extended Data Fig. 9**, **Fig. 2c, d**). This observation suggested that the probe primarily entered the animals through their mouth and then diffused to tissues that were in the proximity. The blue emission channel corresponding to the PI(4,5)P2-bound probe channel showed a pattern around the pharynx for the *gqIs25* strain (**Fig. 2d**) which could be identified as the 'nerve ring' which is a bundle of neurons that form a ring-like assembly around the pharynx (**Fig. 2a, b, d**). 3D reconstructions were used to generate a 360° view image that reconfirmed that the blue emission was significantly brighter in the nerve ring (**Fig. 2d, Video-3**) and distinguishable from the background (**Fig. 2c**). Emission from the nerve ring was observed in all the *gqIs25* worms that were imaged (*n*=18). For wild-type worms (*N2* strains), that have endogenous PI(4,5)P2 levels in neurons, the emission intensity from the nerve ring was lower (**Video-4**) than the intensity obtained for the *gqIs25* worms as expected and was observed in 75% of the worms that were imaged (**Fig. 2c,d**). Intensity analysis of the images indicated that the absolute blue channel emission intensities from the nerve ring were 40% lower in the *N2* strain compared to the *gqIs25* strain (**Fig. 2e**). The average ratio of the blue channel emission intensity from the nerve ring and background was also significantly higher for the transgenic strain by 28% when compared to the wild-type strain (**Fig. 2f**). These results distinctly proved that **MFR-12aa** was both a cell and tissue-permeable, PI(4,5)P2 selective and sensitive probe that could image PI(4,5)P2 in living cells and importantly in

vivo in a multicellular organism. With this validation we next proceeded to visualize PI(4,5)P2 dynamics in the context of GPCR signaling.

Timing PI(4,5)P2 dynamics during GPCR signaling in a cell line

With the PI(4,5)P2 sensitive and selective, small-size, cell-permeable probe we next asked if the marked difference in physiological responses to hallucinogenic versus non-hallucinogenic ligands of the 5-HT_{2A} receptor could be traced back to one of the earliest molecular events in the signaling response to these ligands, i.e. hydrolysis of PI(4,5)P2 when an agonist binds to a Gq-coupled GPCR. We focused on the 5-HT_{2A} receptor, which upon binding its natural ligand, serotonin (5 hydroxytryptamine, 5-HT), activates PLC mediated hydrolysis of PI(4,5)P2 into IP3 and diacylglycerol (DAG) (**Extended Data Fig. 10)**. The 5-HT_{2A} receptor is also one of the primary targets for serotonergic psychedelics, and is thought to contribute to the diverse behavioral and physiological effects of these potent compounds. In this regard, the 5-HT_{2A} receptor provides a platform to assess the earliest lipid signaling signatures that can arise in response to the endogenous ligand, serotonin; a potent serotonergic psychedelic, the hallucinogenic agonist 2,5-dimethoxy-4-iodoamphetamine (DOI); or a non-hallucinogenic agonist Lisuride.

For the first set of experiments, HEK293T cells over-expressing 5-HT_{2A} receptor-eGFP were used. [29] The experimental workflow involved incubating living cells with the **MFR-12aa** probe, setting up the cells on a fluorescence confocal microscope stage and collecting time lapse images at every 5 s. The ligands were added after 60 s of collection of basal fluorescence emission, followed by ligand removal at 210 s to monitor the re-synthesis of PI(4,5)P2 at the membrane. The details of the experimental parameters are provided in the methods section.

Addition of 5-HT to living cells, resulted in 25% depletion in the fluorescence signal of the PI(4,5)P2 bound probe blue emission channel compared to the initial time point (**Fig. 3b,c, Video-5)**. The extent of depletion observed with 5-HT should include the effect of almost simultaneous replenishment of PI(4,5)P2 on the membrane via kinase activity, which can be significantly fast during receptor-mediated signaling processes.[10] In order to validate this point, we added a kinase inhibitor wortmannin (WMN, 10 µM) along with 5-HT. WMN, when applied at ~ 10 µM levels can inhibit the re-synthesis of PI(4,5)P2 from PI(4)P in the plasma membrane.[30,31] Addition of 5-HT+WMN to living cells, resulted in 50% depletion in the fluorescence signal of the PI(4,5)P2 bound probe blue emission channel compared to the initial time point (**Fig. 3a, b, d, Video-6**). A control experiment with only WMN showed no depletion in the fluorescence intensity indicating that the depletion was specific to the loss of PI(4,5)P2 from the cell membrane upon the binding of 5-HT to the 5-HT_{2A} receptor (**Video-5**). Notably, upon ligand wash for the 5-HT+WMN treated cells, we observed a compensation of the depleted signal from the plasma membrane (**Fig. 3a, b, d, Video-6**) which demonstrated the reversibility

of the probe response and its distinct ability in tracking PI(4,5)P2 dynamics in living cells. The signal intensity, however, did not recover back to the original level which could be due to very little loss, if any, during multiple washing steps. This was also reflected in the 5-HT treated cells in which the signal did not recover upon wash. No significant loss in fluorescence intensity across the plasma membrane was observed in the case of vehicle-treated cells, when monitored for the same time duration precluding any photo-damage of the probe and establishing that **MFR-12aa** was photo-stable (**Fig. 3b, Video-6**). Next, we proceeded to visualize PI(4,5)P2 dynamics in response to a hallucinogenic versus a non-hallucinogenic agonist of the 5-HT_{2A} receptor.

DOI the hallucinogenic agonist, has a higher affinity to the 5-HT_{2A} receptor, with respect to the endogenous ligand 5-HT.[32] Upon addition of DOI to living cells followed by time-lapse imaging, a ~ 50% depletion of the blue channel emission of the probe was observed (**Fig. 3e, g, h**). The PI(4,5)P2 depletion response was significantly larger than that observed in the case of 5-HT stimulation alone and comparable to the stimulation by 5-HT with WMN (**Fig. 3b, g**). For, DOI and 5-HT+WMN, the signal from the blue channel decreased steadily till 95 s post ligand addition and then plateaued. On the other hand, stimulation with Lisuride, a non-hallucinogenic agonist, that binds the receptor with comparable affinity as DOI,[33] could bring about faster PI(4,5)P2 depletion within 75 s, reaching a similar plateau as that of DOI or 5-HT+WMN (**Fig. 3g**, **Extended Data Fig. 12**). Surprisingly, we observed no replenishment of PI(4,5)P2 upon washing the agonist in case of DOI-treated cells (**Fig. 3e, g, h, Video-7**) while the Lisuride treated cells afforded recovery of the blue emission intensity of the probe upon agonist washing, indicating PI(4,5)P2 replenishment within the timescale of the imaging experiment **(Fig. 3f, g, i, Video-7**). The result was robust and reproducible and indicated significant ligand-specific differences in PI(4,5)P2 temporal dynamics within 50-100 s post agonist addition (**Extended Data Fig. 12a**).

To test whether these early signaling event differences propagated to downstream processes, we independently monitored two downstream events which follow the action of PLC: 1. Receptor, 5-HT_{2A} receptor-eGFP, endocytosis which occurs almost immediately following ligand-binding;[29] 2. Amounts of inositol-monophosphate (IP1), a stable metabolite of IP3. Additionally, the levels of diacylglycerol (DAG), the product of PI(4,5)P2 depletion on the cell membrane were also measured.

When 5-HT was added to the cells, 5-HT_{2A} receptors internalized within a time frame of 110-115 s (**Extended Data Fig. 11, Video-8**), validating our probe response data depicting PI(4,5)P2 hydrolysis saturation within a similar time range (105-115 s) (**Fig. 3b**). In the case of 5-HT+WMN, the extent of receptor internalization was similar depicting an unbiased response of 5-HT towards 5-HT_{2A} receptor internalization, even in the presence of WMN (**Extended Data Fig. 11e, f**). In a key observation, the difference in PI(4,5)P2 depletion rates were also reflected in the rates of receptor endocytosis, with Lisuride showing faster receptor internalization than DOI (**Extended Data Fig. 11c-f, Video-9, Extended Data Fig. 12**). Replenishment of the GFP-tagged 5-HT_{2A} receptor back to the plasma membrane at the end of the stimulation, has been reported

to be a rather slow process (120-180 min)[34] and thus mirroring the replenishment, in this case, was not possible.

Next, IP1 production in DOI and Lisuride stimulated HEK-293-5-HT_{2A} receptor-eGFP cells, was examined using ELISA (**Extended Data Fig. 13**). End-stage IP1 and DAG levels for Lisuride stimulated cells remain lower in magnitude across the doses and time points tested, as compared to DOI. These results plausibly indicate conversion of IP1 and DAG into replenishing PI(4,5)P2 pools back to the cellular membranes, in line with earlier reported observations.[35] Overall our results indicate that the **MFR-12aa** probe can time differences in one of the earliest signaling events post-ligand binding to a GPCR and that these early time differences are robust and propagate through downstream signaling paths. We next investigated whether the differences observed in PI(4,5)P2 dynamics in the 5-HT_{2A} receptor overexpression cell model could be observed in primary neurons which are the actual site of action for these signaling processes.

Tracking temporal PI(4,5)P2 dynamics in primary cortical neurons using MFR-12aa.

Successful demonstration of the **MFR-12aa** probe toward timing and tracking PI(4,5)P2 dynamics in a 5-HT_{2A} receptor expressing stable cell line, encouraged us to test the probe in the context of primary cortical neurons expressing endogenous levels of 5-HT_{2A} receptor in the cell body and neurites.[36] Primary neurons upon incubation with 1 µM of **MFR-12aa** showed blue/bound probe emission from the membrane of the cell body as well as the neurites (**Fig. 4a-d, Extended Data Fig. 14**), within 5 min of direct incubation.[37] This result indicated the distinct ability of the probe to directly permeate not only cultured cells but also primary neurons, which is a rare feature in molecular probes.

Upon stimulation with 5-HT alone, we observed an ~8 % greater depletion in the PI(4,5)P2 bound probe blue emission from the neurites (26 % depletion) in comparison to the cell body (18 % depletion) (**Fig. 4b, e-h; Video-10**). The differential depletion might be attributed to the higher expression of the 5-HT_{2A} receptor in the neurites, and provide the possibility that the probe could detect for local cellular differences in active receptor signaling pools in neurons.[38] The extents of signal depletion were comparable to 5-HT mediated stimulation alone in the HEK293-5-HT_{2A} over-expression system (25% depletion) (**Fig. 3b, c**). In the case of DOI, we observed a 52% depletion of the probe response from the neurites and 31% depletion from the cell body that were significantly higher as compared to 5-HT stimulation (**Fig. 4c, e-h, Video-11**). On the other hand, in the case of Lisuride-treated primary neurons (**Fig. 4d, e-h, Video-11**), the depletion of signals from the neurites was 42% and cell body was 22% which was lower than that of DOI stimulated neurons, but higher than that evoked by 5-HT stimulation. To illustrate the differential temporal effects of hallucinogenic versus non-hallucinogenic agonists, DOI and Lisuride, snapshots from the early time points have been shown

in **Extended Data Fig. 15.** Together the data distinctly provide evidence for the significantly longer-lasting effects of DOI, the potent hallucinogenic agonist, in comparison to Lisuride, the non-hallucinogenic agonist, at the very earliest stages of signaling events like PI(4,5)P2 depletion.

These findings provide evidence for distinct signaling signatures evoked by hallucinogenic versus non-hallucinogenic 5-HT_{2A} receptor agonists at the earliest stages of signal initiation, uncovered through visualization of the differential rates of PI(4,5)P2 hydrolysis revealed by our probe. These unique results provide evidence of the heterogeneity in signaling to distinct ligands at the same receptor, not only in terms of the nature of time course, but also the manner of signal activation. Our results from cell lines and primary neurons, show that our cell-permeable reversible probe can discern subtle PI(4,5)P2 dynamic signatures in living systems.

Perspective

It is well-established that different ligands of the same Gq-coupled GPCR evoke diverse physiological responses; yet, a key unanswered question is if these signaling outcomes are linked to early-time point differences at the signal initiation stage. To address this question, we need to time early molecular steps that occur within seconds of ligand binding. However, tracking seconds-minute temporal differences in signal transduction, live, has been a significant challenge owing to the lack of apt chemical tools. There is a critical need to reversibly and non-invasively track specific phosphoinositides which are amongst the first molecules at the cell membrane that respond to and mediate signals following the binding of a ligand to a Gq-coupled GPCR. We have addressed this challenge by developing a peptide-based, cell-permeable, ratiometric fluorescent probe **MFR-12aa**. In vitro, in cell, and in vivo studies validated that the probe could selectively and sensitively detect PI(4,5)P2, the phosphoinositide that mediates Gq-coupled GPCR signaling. The probe has two key salient features: First, reversibility which was introduced into the probe design by strategically converting non-covalent interactions between the peptide-binding scaffold and PI(4,5)P2 into a fluorescence response; Second, photo-stability, achieved via a fluorene-based fluorophore. These features play a pivotal role as we interrogated whether the responses of a hallucinogenic versus a non- hallucinogenic agonist of the serotonergic receptor showed any differences in PI(4,5)P2 mediated signaling within seconds of agonist-receptor binding. In the central result of this report, we show that the probe could indeed time differences in PI(4,5)P2 depletion, an early time point signaling event that occurs upon ligand binding to a Gq-coupled GPCR, and capture differential temporal dynamics of PI(4,5)P2 for a hallucinogenic versus a non-hallucinogenic agonist of the 5-HT_{2A} receptor. Given the highly differential behavioral and physiological outcomes when the 5-HT_{2A} receptor is stimulated by hallucinogenic versus non-hallucinogenic agonists, our results provide evidence of distinctive changes in PI(4,5)P2 depletion, that are revealed at the early stages of ligand-receptor

interaction. This result opens the floodgates for applying short-peptide based cell-permeable lipid probes for tracking the spatiotemporal dynamics of these critical signal mediators. The power of this tool lies in uncovering the earliest of signaling signatures that may underlie the distinctive physiological and behavioral outcomes that arise in responses to diverse ligands of Gq-coupled receptors.

Figures

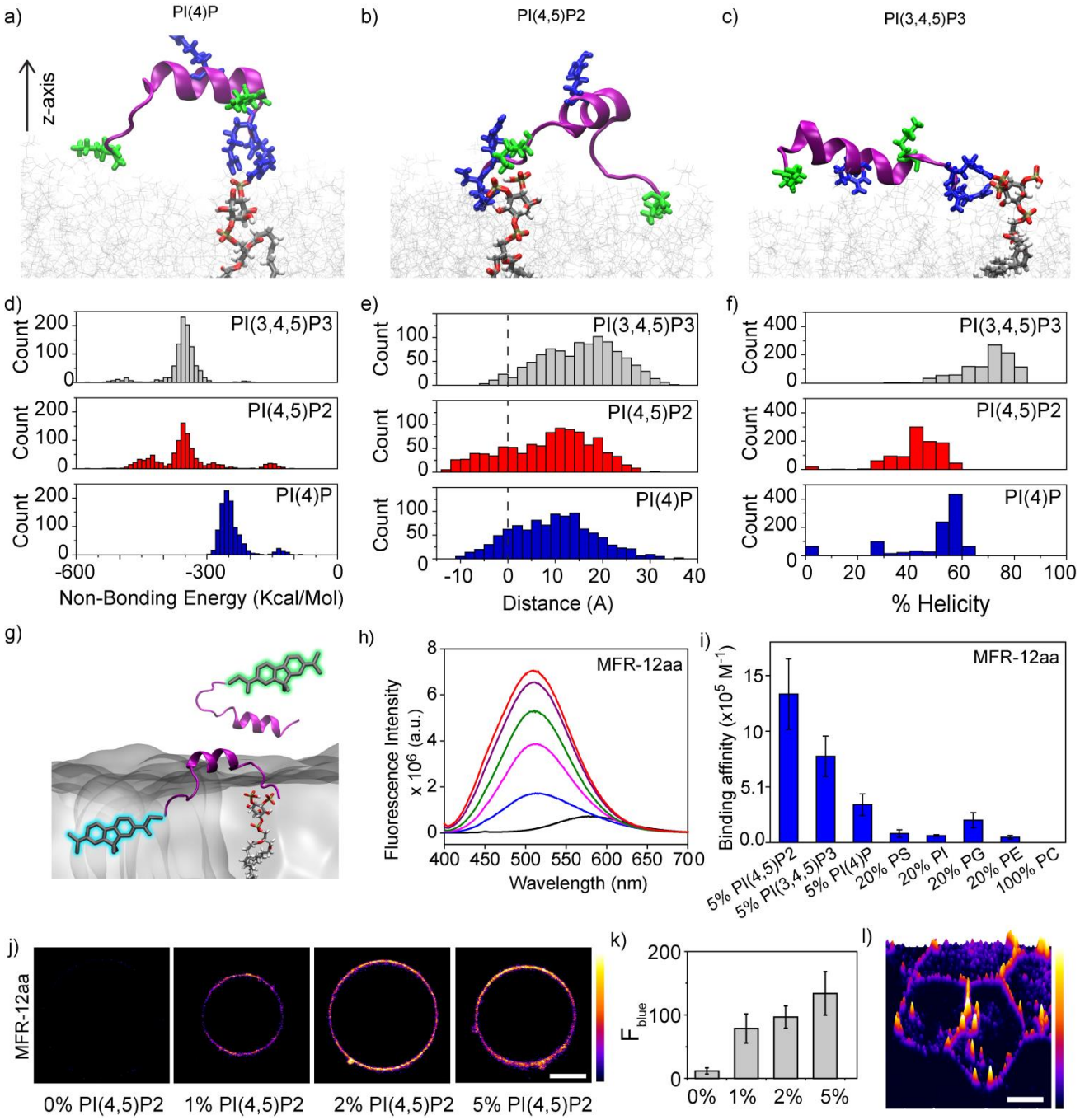

Fig. 1 | A peptide-based ratiometric fluorescent probe detects PI(4,5)P2 selectively. Snapshots from MD simulations showing Gel-20aa-phosphoinositide interaction (phosphoinositide gray licorice, O-atoms in red) in a PC (gray lines) membrane bilayer: (a) PI(4)P, (b) PI(4,5)P2, and (c) PI(3,4,5)P3. The peptide backbone is in magenta and cationic amino acids are shown in blue (Arg) and green (Lys). (d) Distributions of non-bonding energies for binding of the Gel-20aa

peptide to phosphoinositide headgroups. (e) Distributions of the distance between the N-terminus amine group of Gel-20aa and the membrane surface (dashed line) along the z-axis as shown in Fig. 1a. (f) Distributions of helicity content of the Gel-20aa peptide upon binding to phosphoinositide headgroups. All distributions shown in d-f have been calculated from 200 ns MD simulation trajectories. (g) Schematic depiction of sensing strategy used for PI(4,5)P2 detection. (h) Fluorescence response of **MFR-12aa** (1 µM) depicting a blue shift in emission maxima with increasing concentrations (0, 5, 10, 25, 71, and 114 µM) of 5% PI(4,5)P2-PC SUVs, λ_{ex} 390 nm. (i) Bar plot (mean ± SEM., *N* = 3) comparing the association constants (K_a) of **MFR-12aa** toward various PLs, derived from fluorescence titrations. (j) Confocal images of GUVs containing PI(4,5)P2 (x% where x = 0, 1, 2, 5) in PS (20%)-PC (80-x%) incubated with **MFR-12aa** (200 nM). (k) Bar plots representing average intensity along the perimeter of GUVs obtained from calculations on 10 vesicles. Error bars represent SEM, *N*=3. (l) 3D intensity plot generated from confocal microscopy image of living HEK293T cells incubated with **MFR-12aa** (5 µM) for 15 min at room temperature. Confocal images (j, l) were recorded in blue channel (480-520 nm, λ_{ex} 780 nm) and are representative of 3 independent experiments. Scale bars, 10 µm.

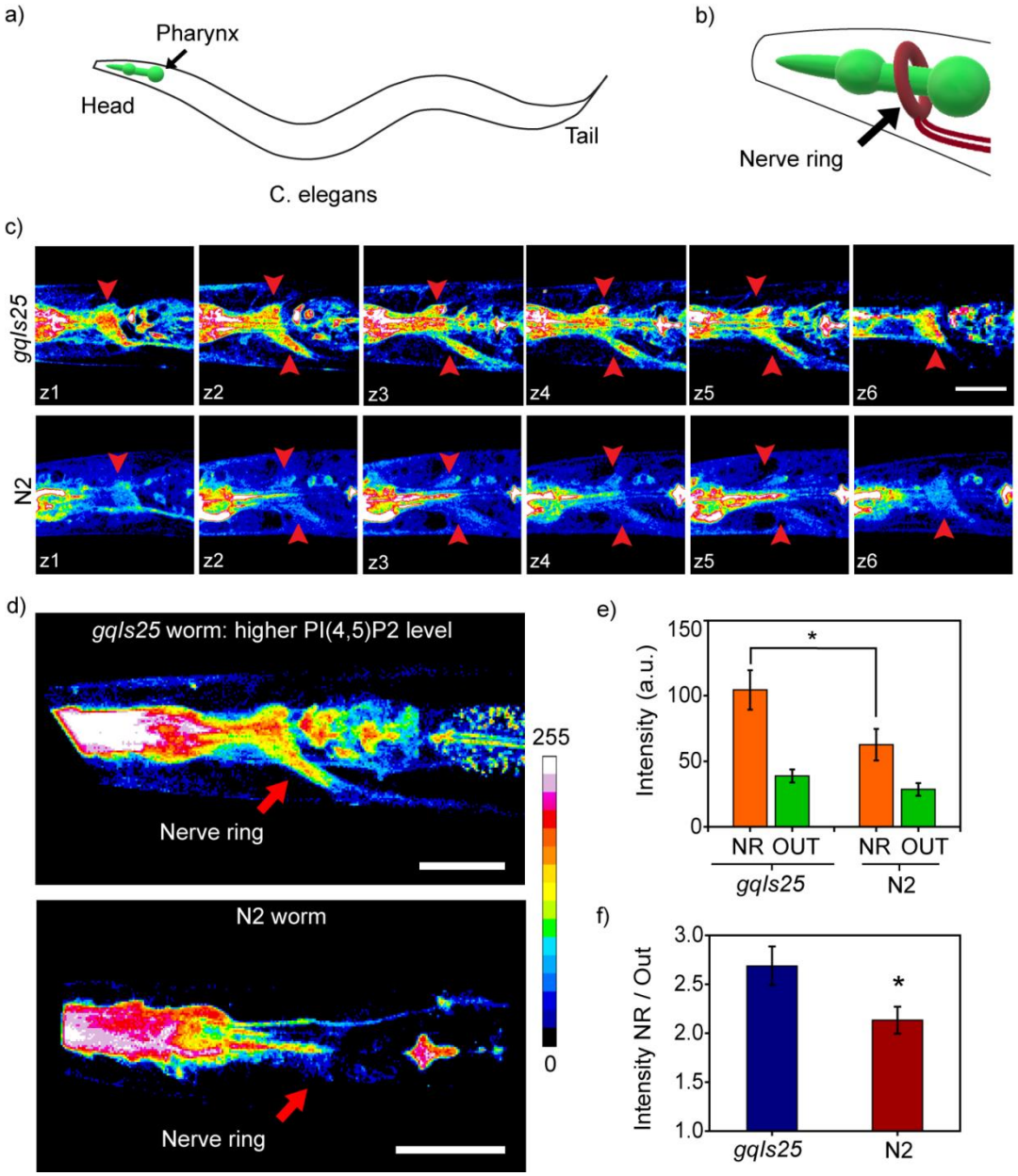

Fig. 2| MFR-12aa images PI(4,5)P2 in a multicellular model system. (a) Diagram of *C. elegans* with pharynx region highlighted in green. (b) Enlarged diagram showing the nerve ring around the pharynx in the head region. (c) Confocal z-sections (*z1-z6*) of the head region of a PI5K overexpressing transgenic (*gqIs25*) worm (top panel) and a wild type *N2* worm (bottom panel). Images were acquired in the blue channel (480-520 nm) and the regions identified as the sections of the nerve ring are pointed with red arrows. (d) 3D reconstructions from the confocal images recorded at the head region of a PI5K overexpressing transgenic (*gqIs25*) worm (top) and wild type worm (bottom). (e) Bar plot representing raw fluorescence intensities from a region of interest (ROI) selected within the area identified as nerve ring (NR) and an ROI of same area chosen within the tissue section which is away from the pharynx and the nerve ring (OUT) for transgenic

and wild type animals. (f) Ratio of intensities in the NR with respect to that of ROI outside NR. Error bars represent SEM. Unpaired Student's *t* test, *n*=18 for transgenic and *n*=14 for *N2*, from 3 independent experiments*, *p=0.04, **p=0.03*. Scale bar, 10 µm.

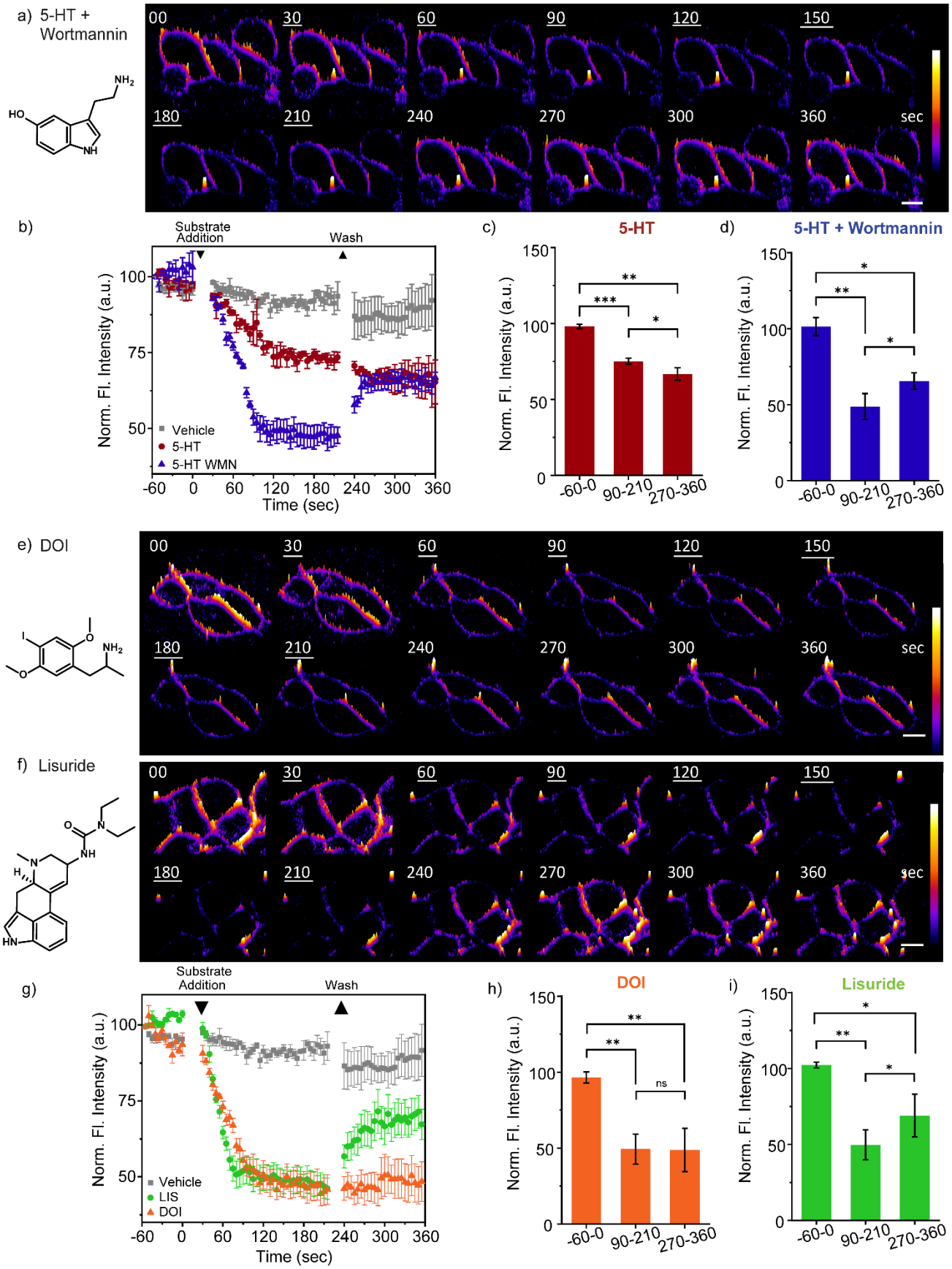
a) 5-HT + Wortmannin
00
30
60
90
120
150
180
210
240
270
300
360
sec
b)
Substrate Addition
Wash
Norm. Fl. Intensity (a.u.)
Time (sec)
Vehicle
5-HT
5-HT WMN
c)
5-HT
d)
5-HT + Wortmannin
-60-0
90-210
270-360
e) DOI
f) Lisuride
g)
LIS
DOI
h)
DOI
i)
Lisuride
ns

Fig. 3| Neurotransmitter, hallucinogen, and non-hallucinogen mediated PI(4,5)P2 dynamics in live 5-HT$_{2A}$ receptor over-expressing HEK293 cells. Confocal time lapse imaging of cells incubated with **MFR-12aa** (5 µM) using two-photon excitation λ_{ex} 780 nm, λ_{em} 480-520 nm. Scale bar, 10 µm. Time trace for a single z-slice in 3D intensity plot representation during stimulation of cells with: (a) 5-HT (10 µM) and WMN (10 µM); (e) DOI (10 µM); and (f) Lisuride (10 µM). Data were acquired for unstimulated cells (1 min, -60-0 s), followed by stimulation via ligand addition at 0 s (3 min, 30-210 s) and ligand removal via replacement with fresh media at 210 s (3 min, 240-360 s). Time points indicating the start and end of stimulation are underlined. Data depicted is representative of three independent repeats for each experiment. Time traces of fluorescence intensity, calculated by normalizing the fluorescence intensity, depicting differential rates of ligand dependent PI(4,5)P2 hydrolysis and replenishment for: (b) 5-HT (maroon), 5-HT + WMN (blue), and vehicle (0.01% DMSO) (gray), and (g) DOI (orange), Lisuride (green), and vehicle (0.01% DMSO) (gray). Fluorescence intensity in the blue channel in the selected ROI of the membrane from individual experiment was averaged and normalized to the initial intensity (t= -60s) of the same experiment. Mean of these averaged values from three independent experiments are plotted as a time trace until 360 s of image acquisition. Error bars represent standard error of mean from three individual experiments. Normalized fluorescence intensity bar plots representing average intensity values for the time intervals -60-0 s, 90-210 s, 270-360 s calculated from time lapse images of cells treated with: (c) 5-HT (10 µM); (d) 5-HT (10 µM) and WMN (10 µM); (h) DOI (10 µM); and (i) Lisuride (10 µM). Ligand addition has been marked at 0 s and washed at 210 s. Error bars represent standard error of mean from three individual experiments (N = 3; vehicle, n = 46; 5-HT, n = 46; 5-HT and WMN, n = 47; DOI, n = 41; LIS, n = 47); ** p = 0.02, ** p = 0.01, *** p = 0.001* using Student's *t*-test.

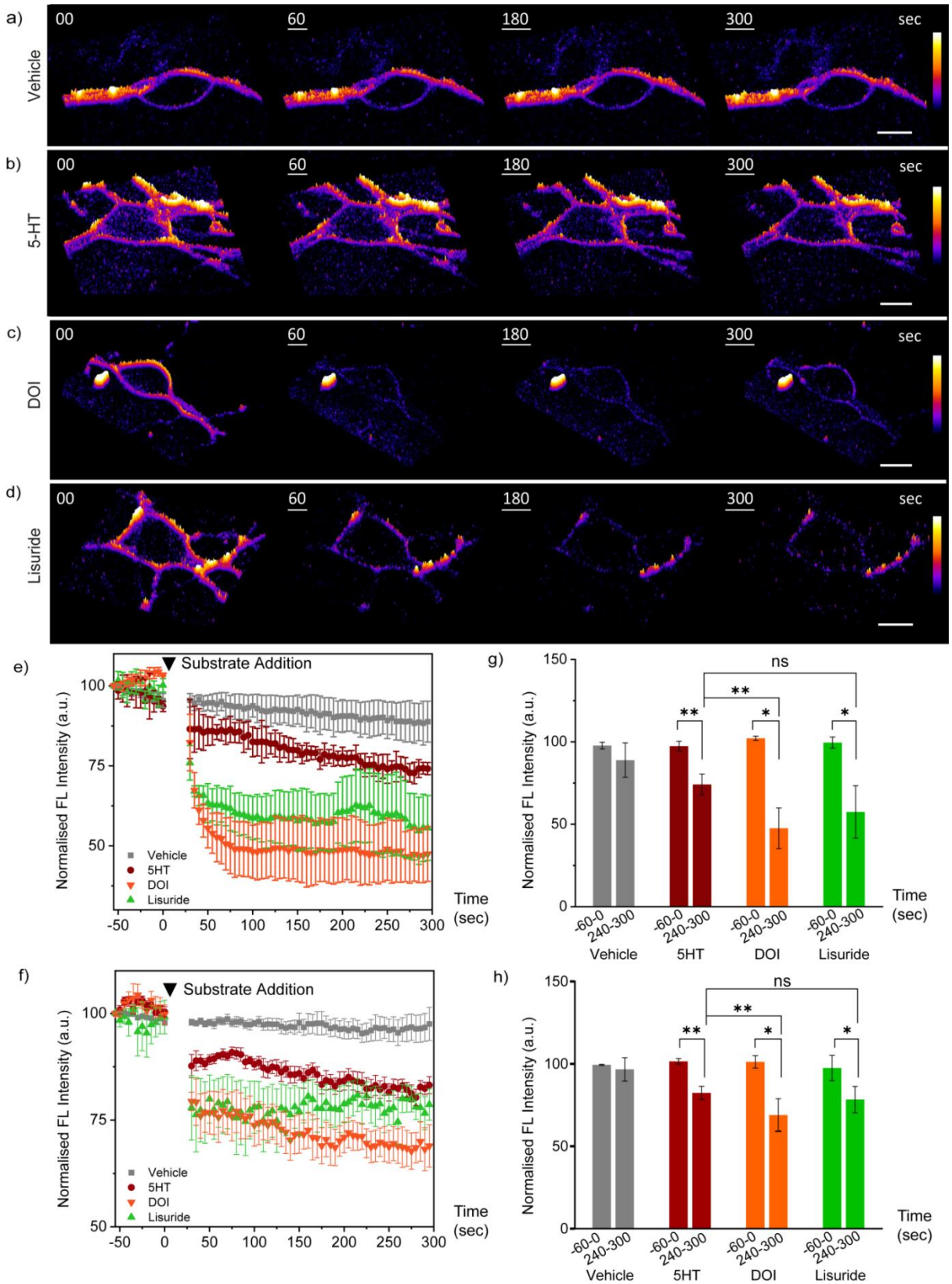
a)
Vehicle
00
60
180
300
sec
b)
5-HT
c)
DOI
d)
Lisuride
e)
Substrate Addition
Normalised FL Intensity (a.u.)
Vehicle
5HT
DOI
Lisuride
Time (sec)
f)
g)
ns
**
*
-60-0
240-300
h)

Fig. 4| Localized dynamics in cortical neurons in presence of neurotransmitter, hallucinogen, and non-hallucinogenic agonists. (a-d) Confocal time lapse imaging of rat primary cortical neurons incubated with **MFR-12aa** (1 µM), using two-photon excitation at λ_{ex} 780 nm, λ_{em} 480-520 nm. Time trace for a single z-slice in 3D intensity plot representation during stimulation of cells with: (a) vehicle (0.01% DMSO); (b) 5-HT (10 µM); (c) DOI (10 µM); and (d) Lisuride (10 µM). Data were acquired for unstimulated cells (1 min, t= -60-0 s), followed by stimulation via ligand addition at 0 s (5 min, 0-300 s). Time points indicating stimulation are underlined. *N*=4. (e,f) Time traces of fluorescence intensity depicting differential rates of ligand dependent PI(4,5)P2 hydrolysis for: 5-HT, DOI, Lisuride, and vehicle (0.01% DMSO), for: (e) neurites; and (f) neuron cell body. Fluorescence intensity in the blue channel in the selected ROI on the membrane from individual experiment was averaged and normalized to the initial intensity (t=-60s) of the same experiment. Mean of these averaged values from three independent experiments are plotted as a time trace until 300 s of image acquisition. Time points indicating ligand addition are pointed by downward arrowheads. Normalized fluorescence intensity bar plots representing average intensity values for the time intervals -60-0 s, and 240-360 s calculated from time lapse images of cells treated with 5-HT (10 µM), DOI (10 µM), Lisuride (10 µM), and vehicle for (g) neurites and (h) neuron cell body. Error bars represent SEM, *N=4* (cell body: *n* = 3-5: cell processes: *n* = 11-15); * *p* = 0.02, ** *p* = 0.01, ****p*=0.001 using Student's t-test, scale bar, 10 µm.

Methods

1. Simulation system Preparation

Simulations were performed using the NAMD 2.11 simulation package. Initial peptide coordinates were obtained from RCSB protein data bank, PDB ID 1SOL. The lipid bilayer model was generated by VMD software using the 'Membrane Builder' plug-in. A membrane of 100 Å x 100 Å dimension composed of POPC was built using CHARMM36 force field. The coordinate files for PI(4)P (SAPI14), PI(4,5)P2 (SAPI24) and PI(3,4,5)P3 (SAPI33) were taken from the "CHARMM-GUI Archive - Individual Lipid Molecule Library". In each case, a single PI(4)P/ PI(4,5)P2/ PI(3,4,5)P3 molecule was inserted into one leaflet of the POPC membrane. For each phosphoinositide we generated a model comprising of one phosphoinositide molecule per 135 POPC molecules which corresponded to 0.74 mol% of phosphoinositide on that leaflet. The missing atoms were added using CHARMM36 force field for lipids as well as peptide structure and psf files were generated from the pdb file inputs. The pdb and psf files were used for equilibration, minimization, and production run. After generation of the lipid bilayers, the model systems were solvated in a water box followed by neutralization and ionization with Na^+ and Cl^- ions maintaining the NaCl concentration at 120 mM. The equilibrated peptide was incorporated into the system after the lipid bilayer was equilibrated. All the simulations were run with a periodic simulation box condition.

2. Simulation details

Equilibration of the membrane. Membrane equilibrations were performed using the NAMD simulation package and CHARMM36 force field. The lipid bilayer was energy minimized and equilibrate through 3 steps – a) 10000 steps of minimization followed by 0.5 ns equilibration at 300 K keeping everything free except the lipid tails fixed; b) Repetition of minimization and equilibration steps keeping all non-hydrogen atoms under harmonic constrains (changing from higher to lower) both lipid tails and headgroups, water and ions free. c) The whole system was equilibrated again at 300 K for 1 ns setting all atoms free.

Equilibration of the peptide. The peptide structure was decided on the basis of previously reported literature which proposed that, upon binding to PI(4,5)P2 the Gel-20aa sequence formed a helix, imposing a major conformation change in the protein, displacing it from actin filaments.[39] The structure of the 20aa peptide obtained from Protein Data Bank (PDB ID: 1SOL) which was acquired via an NMR experiment in presence of helix inducing solvent TFE.[23] The peptide PDB structure had a $–COO^-$ group at the C-terminal. As the experiments were performed with $–CONH_2$ terminal peptides, the C-terminal capping was modified to $–CONH_2$ by using a patch in VMD before equilibration and minimization. The peptide was incorporated into a modeled

water box generated via VMD. The box size was maintained such that the distance between the peptide and its periodic image remained more than 28 Å in all directions. The solvent box was neutralized by adding the requisite number of Na^+ and Cl^- ions and total NaCl concentration was maintained to be 120 mM. The system was subjected to the following minimization steps: (a) keeping the non-hydrogen heavy atoms in the peptide fixed with harmonic constraints of 25 and 12 kcal/mol/$Å^2$ on the peptide heavy atoms; (b) The minimization steps were followed by heating the system from 0 K to 300 K in two steps: (1) steady increment of temperature in steps of 6 K/1 ps from 0 K to 300 K; (2) equilibration at 300 K for 50 ps keeping the protein heavy atoms fixed; (3) repeating the heating and equilibrium steps keeping the heavy atoms under harmonic constraints of 25 kcal/mol/$Å^2$. The harmonic constraints were gradually released in NPT (1 atm pressure and 300 K temperature) equilibration steps of 1 ns. For the shorter peptide, Gel-12aa, structure was generated by truncating the equilibrated 20aa peptide structure after the 12th amino acid from the C-terminus. Then the N-terminus was capped with $–CONH_2$. Rest of the steps were done following the above-mentioned procedures.

Insertion of the peptide onto the lipid bilayer and simulation. The equilibrated peptide was aligned with the equilibrated membrane containing PI(4,5)P2 in two different orientations: a) keeping the C-terminus close to the headgroup, and b) keeping the N-terminus close to the headgroup. In both cases upon running short 100 ns simulations, stable electrostatic contacts were formed between the C-terminus positively charged residues and the phosphoinositide headgroup. Hence, for all following simulations, the C-terminus was placed close to the phosphoinositide headgroup at the starting point of the simulations with the membrane. The peptide-membrane system was re-solvated and ionized with 120 mM NaCl. The whole system was subjected to the following steps– (a) The harmonic constraints were gradually released in five NPT (1 atm pressure and 300 K temperature) equilibration steps of 1 ns each, (b) NPT production runs were carried out for 200 ns. All simulations employed periodic boundary conditions with the PME algorithm describing long range electrostatic interactions. The van der Waals forces were calculated by using a switching function that had 10 Å as the switching distance and 12 Å as the cutoff.

Analysis of simulations was conducted using NAMD. N-terminal dipping, non-bonding energy, and peptide helicity calculations were done on the .dcd files generated after the final NPT production run. For 200 ns trajectories, we have considered 1000 frames for all the calculations. The distance (z-coordinate difference) between the N-terminus amine group of the peptide and the membrane surface, calculated throughout the simulation, determined the peptide's position relative to the membrane, with positive values indicating above-surface placement and negative values indicating penetration into the membrane. The non-binding energies were computed between positively charged amino acid residues on the peptide, which approached within 3

Å of phosphoinositide headgroup and negatively charged phosphate groups on the phosphoinositide headgroup for the calculations.

A summary of simulations performed is provided in **extended data table 1**.

3. Labelling of the peptide with MFR-COOH dye

Synthesis and characterization of the dye and peptides have been mentioned in the supplementary information. Labelling with MFR-COOH dye was performed on the peptides conjugated to beads. Synthesized peptide on beads (20 mg) was coupled with MFR-COOH (3 eq., 0.22 mmol), HATU (3 eq., 0.22 mmol), and N, N-Diisopropylethylamine (DIPEA) (3 eq., 0.22 mmol) by mechanical mixing for 48 h. Labelled peptide on the beads was washed with DMF to remove the excess unreacted dyes and beads were dried under vacuum. Peptide was cleaved from the resin by treating with the cleavage cocktail mentioned previously for 4 h. The resin beads were removed from the mixture and the solution was concentrated under a stream of N_2. The crude peptides were precipitated out in cold methyl tert-butyl ether.

4. Purification and characterization of the MFR probes

MFR labeled peptides were purified on a Varian PrepStar, SD-1 HPLC system, equipped with a Phenomenex Luna® C18(2) (250 x 10 mm) semi-preparative column. Water (solvent A) with trifluoroaceticacid (0.1% v/v) and acetonitrile (solvent B) with trifluoroaceticacid (0.1% v/v) were used as mobile phase and absorption at 220 nm and 390 nm were monitored for product elution. The purification method was set to a gradient flow for 0-5 min: 5% solvent B; 5-60 min: 5-100% solvent B; 60-65 min: 100% solvent B; 65-75 min: 100-5% solvent B; 80 min: 5% solvent B. HPLC fractions were characterized by MALDI-TOF-MS (Bruker UltrafleXtreme, Bruker Daltonics) using HCCA matrix to identify fractions containing the desired product. Pure fractions were evaporated under reduced pressure on a vacuum concentrator (Eppendorf Concentrator Plus, Eppendorf AG, Germany). Purity of the probe was further confirmed by electro-spray ionization liquid chromatography mass spectroscopy (LC-ESI/MS) and MALDI-TOF-MS.

5. Fluorescence titration of the probes with small unilamellar vesicles (SUVs)

All measurements were performed in buffer (20 mM HEPES, 100 mM NaCl, pH 7.4) at 25 °C. Probes (1 µM) were dissolved in buffer and concentrations of the stock solutions were measured using a NanoDrop 1000 spectrophotometer (Thermo Fisher Scientific, Inc.) by monitoring the MFR absorbance at 390 nm (molar absorptivity of MFR at 390 nm = 43000 $M^{-1}cm^{-1}$). Probe solutions (1 µM, 200 µL) were mixed with the SUVs and fluorescence spectra were recorded in a FluoroLog-3 spectrofluorometer (Horiba Jobin Yvon, Inc.) by

excitation at 390 nm. To determine dissociation constants (K_d), probes were titrated against SUVs composed of different phospholipids and F_{480}/F_{580} values were plotted against corresponding phospholipid concentrations. The response curves were fitted to the equation, $(F_{480}/F_{580}) = (F_{480}/F_{580})_{max}/(1+K_d/[phospholipid])+(F_{480}/F_{580})_0$ for ratiometric fitting for **MFR-20aa** and $F= (F_{max}-F)_0/(1+K_d/[phospholipid])+F_0$ for turn on fitting for **MFR-12aa** and K_d values were obtained from the fits. For comparison studies, fluorescence spectra were recorded with the probes (1 µM) in the presence of either SUVs or IP3.

6. Confocal imaging of the probes on giant unilamellar vesicles (GUVs)

GUVs were incubated in 200 nM probe solution and allowed to settle for 10 min. Imaging was done on a Ziess 710 multiphoton confocal microscope. MaiTai Titanium Sapphire Crystal laser was set at 780 nm and power adjusted optimally. GUV imaging was done on a 40x water immersion objective with N/A of ¼. A suitable position with spatially oriented GUV was selected and imaged. λ_{ex} was set at 780 nm and image were procured. Blue (bound) 480-520 nm channel images have been shown in Fig. 1j. Laser power and detector gain were adjusted in order to avoid signal saturation at the highest PI(4,5)P2 concentration imaged. All GUV images were taken under identical laser power and detector gain. Confocal images were analyzed using ImageJ (NIH, USA) software and the intensities along the perimeter of the confocal images of the GUVs were measured using a Concentric Circles plugin. Three independent experiments were performed and 10 GUVs were considered for analysis in each experiment.

7. Imaging PI(4,5)P2 in HEK-293 cells

HEK293T cells were cultured in Dulbecco's Modified Eagle Medium (DMEM, SigmaAldrich) high glucose supplemented with fetal bovine serum (10%), Penicillin (50 units/ml) and Streptomycin (50 µg/ml) in T-25 culture plates at 37 °C inside an incubator containing humidified 5% CO_2. For imaging, the cells were seeded on home-made glass coverslip bottomed dishes (35 mm diameter, Tarsons) coated with polylysine (0.1 mg/mL), and incubated at 37 °C under 5% CO_2 for 24 h. Cells plated on glass coverslips were washed with DMEM high glucose, phenol red free medium and incubated at 37 °C with **MFR-12aa** (5 µM in phenol red free DMEM) for 15 min. Following incubation, the cells were washed twice with phenol red free DMEM. λ_{ex} was set

at 780 nm and image was procured in two different channels, blue (bound) 480-520 nm and orange (bound+unbound) 580-620 nm.

8. Imaging phosphoinositides in *C. elegans*

Wild type (N2) and gqIs25 strains of *C. elegans* were grown following standard protocols. All imaging experiments were performed at the young adult stages (between L4 to 1-day adult) of the worms. Before probe incubation worms were washed with Milli-Q water. The washed worms were then transferred into a solution containing **MFR-12aa** (10 µM) in M9 buffer and were allowed to swim freely for 1 h at room temperature. After the incubation, worms were taken out of the probe solution and again washed with water to remove excess probe from the body surface. For confocal imaging, worms were anesthetized with sodium azide solution (30 mM, in M9 buffer, 10 min). The anesthetized worms were placed onto an agar pad (2% low density agar in Milli-Q water) made on a microscope slide and gently covered with a glass cover-slip. The slide containing worms was placed on the microscope stage keeping the cover-slip side facing the microscope objective. Worms were imaged with a 40x water immersion objective upon two-photon excitation at 780 nm using the same instrument settings that were used for cellular imaging with **MFR-12aa**. Optical sections along the z-direction were taken in every 1 µM difference in order to create 3D reconstructions. Confocal images were processed and analyzed using ImageJ software.

9. Imaging phosphoinositide dynamics in HEK293 cells over-expressing 5-HT_{2A} receptor-eGFP

Generation and characterization of the HEK293 cells stably expressing the human serotonin receptor type 2A fused to eGFP (HEK- 5-HT_{2A} receptor-eGFP cells) is described previously.[41] Cells were maintained in DMEM high glucose supplemented with 10% FBS, antibiotic-antimycotic solution and neomycin analogue G418 (1 mg/ml) in T25 culture flasks at 37°C, 5% CO_2. 24 hours prior to imaging studies, cells were seeded (2 x 10^5 cells per well) in 35-mm glass bottom dishes (Nunc). Cells were initially starved with DMEM without FBS supplemented for 4-6 hours incubated at 37 °C. Serum free media was replaced with **MFR-12aa** probe solution (5 µM) in DMEM high glucose, phenol red free medium for 15 min incubated at 37 °C. Probe solution was washed twice with Phenol red free DMEM and imaged on a Ziess 710 Multiphoton Confocal Microscope.

10. Primary Cortical Neuronal cultures

Primary cortical neuronal cultures were established from postnatal day 0 Sprague Dawley rat pups. All experimental procedures were in accordance with the guidelines of the Committee for Supervision and Care

of Experimental Animals (CPCSEA), Government of India, and were approved by the TIFR Institutional Animal Ethics committee.

Imaging dishes were pre-coated 4-6 hours prior to seeding with 0.1 mg/mL Poly-D-Lysine hydrobromide. Under aseptic conditions, pup brains were dissected and placed in Hanks' balanced salt solution supplemented with antibiotic-antimycotic solution. The cortical tissue was dissected and trypsinized for 10 min at 37°C. Thereafter, cells were dissociated by repeated trituration using Minimum Essential Medium Eagle (MEM) containing Hank's Salts, 25 mM HEPES buffer, L-Glutamine and Sodium bicarbonate supplemented with 10% FBS. Cells were then plated ($2x10^5$ cells per well) in DMEM supplemented with 10% FBS at 37°C, 5% CO_2 for 3-4 hrs. After that, the media was replaced to Neurobasal medium, supplemented with 2% B27, 0.5 mM L-Glutamine and antibiotic-antimycotic solution. Half of the medium in the dishes was replaced every alternative day with fresh neurobasal medium containing the supplements mentioned above. Cells were maintained for 7-10 days *in vitro* before use in experiments and experiments were performed when the cultures comprised of 90-95% neurons. For vehicle or drug inductions prior to imaging, Neurobasal phenol red free medium was used. During probe incubation, supplemented neurobasal media was replaced with **MFR-12aa** probe solution (1 µM) in neurobasal, phenol red free medium for 5 mins and incubated at 37 °C. Probe solution was washed twice with phenol red free Neurobasal and imaged on a Ziess 710 Multiphoton Confocal Microscope.

11. Confocal Imaging parameters

Imaging was done on a Ziess 710 Multiphoton Confocal Microscope. MaiTai Titanium Sapphire Crystal laser was set at 780 nm and adjusted to a power of ~ 30 mW on a 10x objective. Cell Imaging was done on a 40x water immersion objective with N/A of ¼. A suitable position with spatially and uniformly distributed cells was chosen on the plate and the best focused z-slice was set. λ_{ex} was set at 780 nm and image was procured in two different channels, blue (bound) 480-520 nm and orange (bound+unbound) 580-620 nm using an external PMT for the transmission image. Three independent experiments were performed and a total of 30-50 cells were considered for analysis. A timeline was followed for capturing the depletion and replenishment response of the probe in a stipulated timeline as mentioned below. Data acquisition was started in a cycle mode of 5 s interval for a total time of 6 min. An initial 60 s (12 frames) was acquired to understand the intracellular/endogenous flux of PI(4,5)P2 dynamics. Acquisition was paused and media was replaced with the respective concentration of the desired ligands. Removal and addition of ligands took around 20-22 s; thus a time delay of 25 s was maintained using a stopwatch, wherein the data acquisition was resumed again. After 180 s of ligand exposure, data acquisition was paused again, (210 s) ligand solution was removed, and fresh media was added. This was repeated twice to ensure complete removal of ligand. Again, data acquisition was

resumed after 30 s (240 s), for an additional time of 2 min. For primary neuronal cells data acquisition was continued until 300 s of ligand exposure.

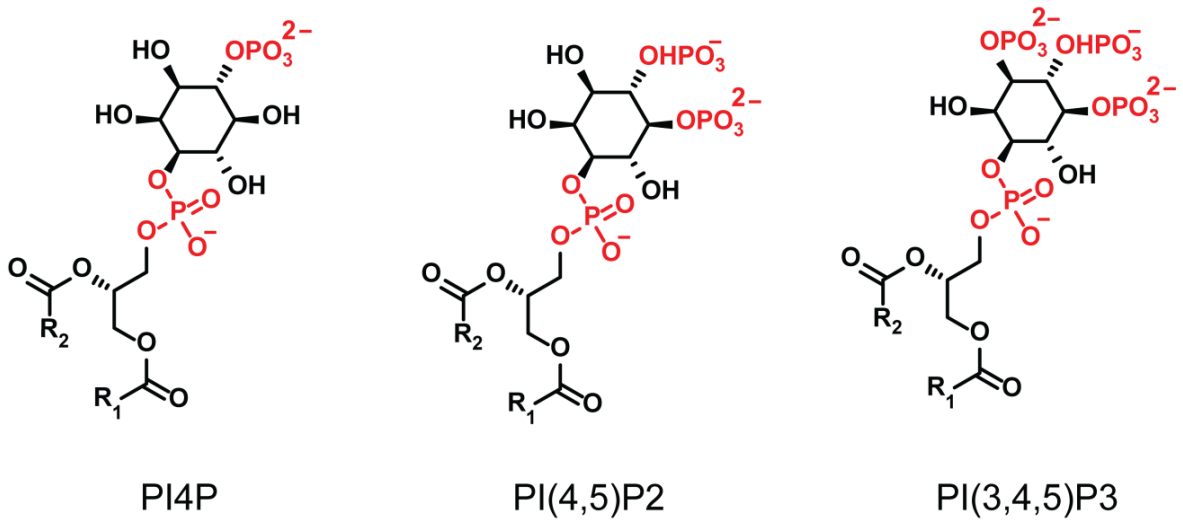

Extended Data Fig. 1| Representative chemical structures of phosphoinositides: phosphatidylinositol-4-phosphate (PI(4)P), phosphatidylinositol-4,5-bisphosphate (PI(4,5)P2), and phosphatidylinositol-3,4,5-trisphosphate (PI(3,4,5)P3). R1 and R2 are stearic acid and arachidonic acid tails.

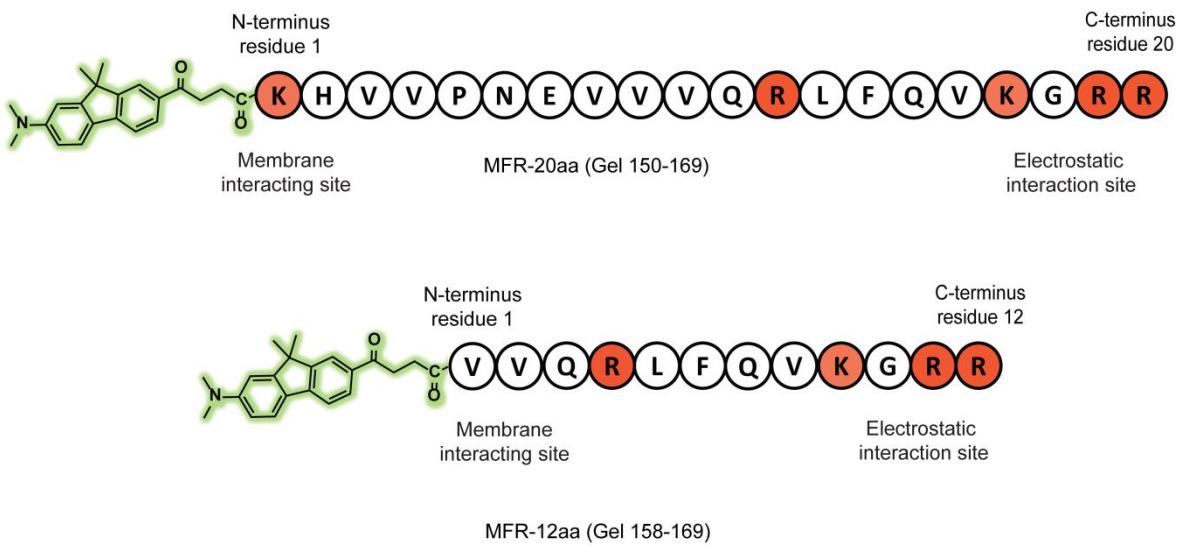

Extended Data Fig. 2| Representative images of the probes **MFR-20aa** (above) and **MFR-12aa** (below). Cationic amino acids have been indicated in orange.

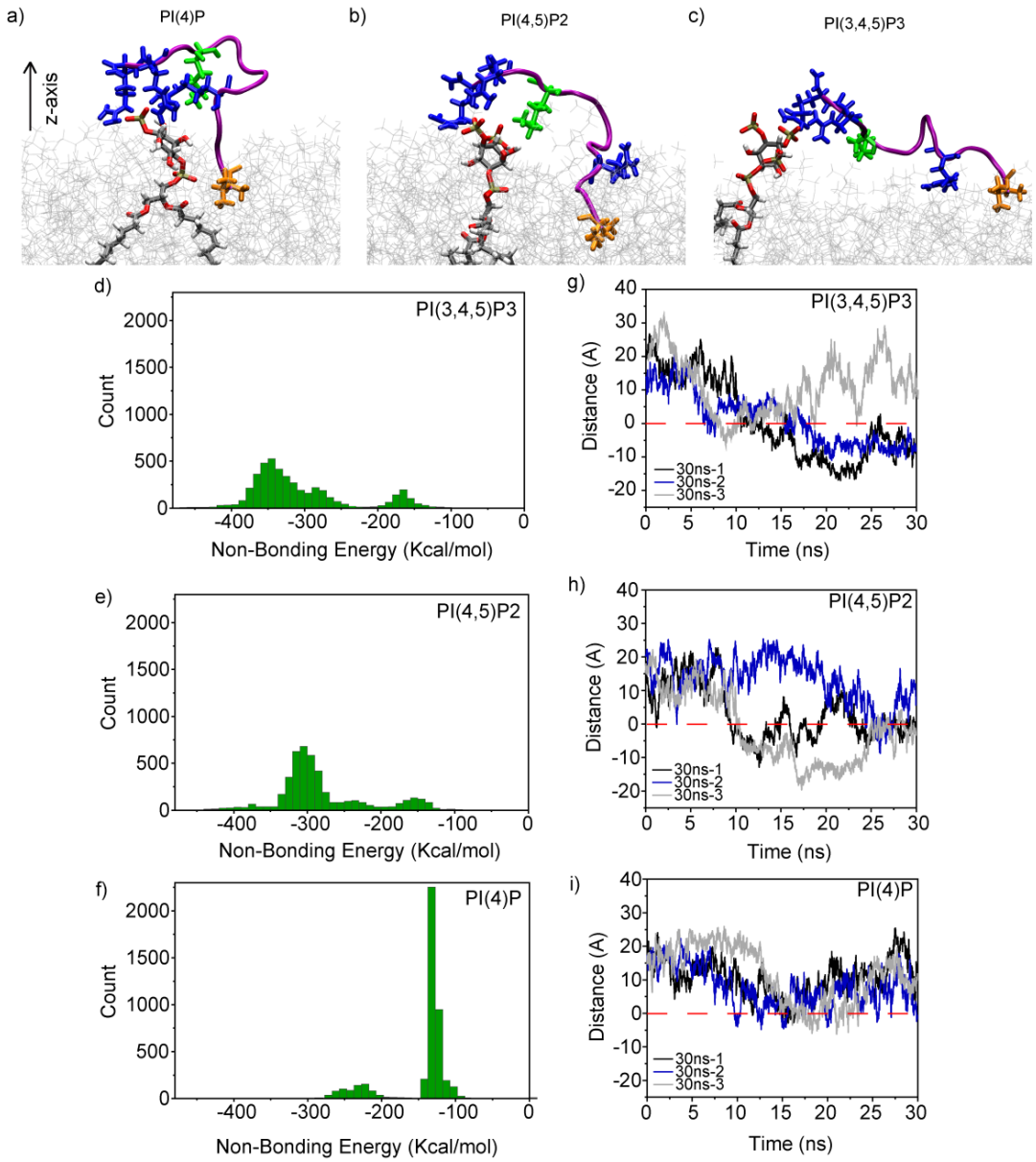

Extended Data Fig. 3| Snapshots from MD simulations showing Gel-12aa-phosphoinositide interactions (phosphoinositide gray licorice, O-atoms in red) in a PC (gray lines) membrane bilayer: (a) PI(4)P, (b) PI(4,5)P2, and (c) PI(3,4,5)P3. The peptide backbone is in magenta and cationic amino acids are shown in blue (Arg) and green (Lys). Distributions of non-bonding energies for binding of the Gel-12aa peptide to (d) PI(3,4,5)P3 (e) PI(4,5)P2, and (f) PI(4)P headgroups. Distributions of the distances between the N-terminus amine group of Gel-12aa and the membrane surface (dashed line) along the z-axis (Ext.Fig.3a) after interacting with (g) PI(3,4,5)P3 (h) PI(4,5)P2, and (i) PI(4)P headgroups.

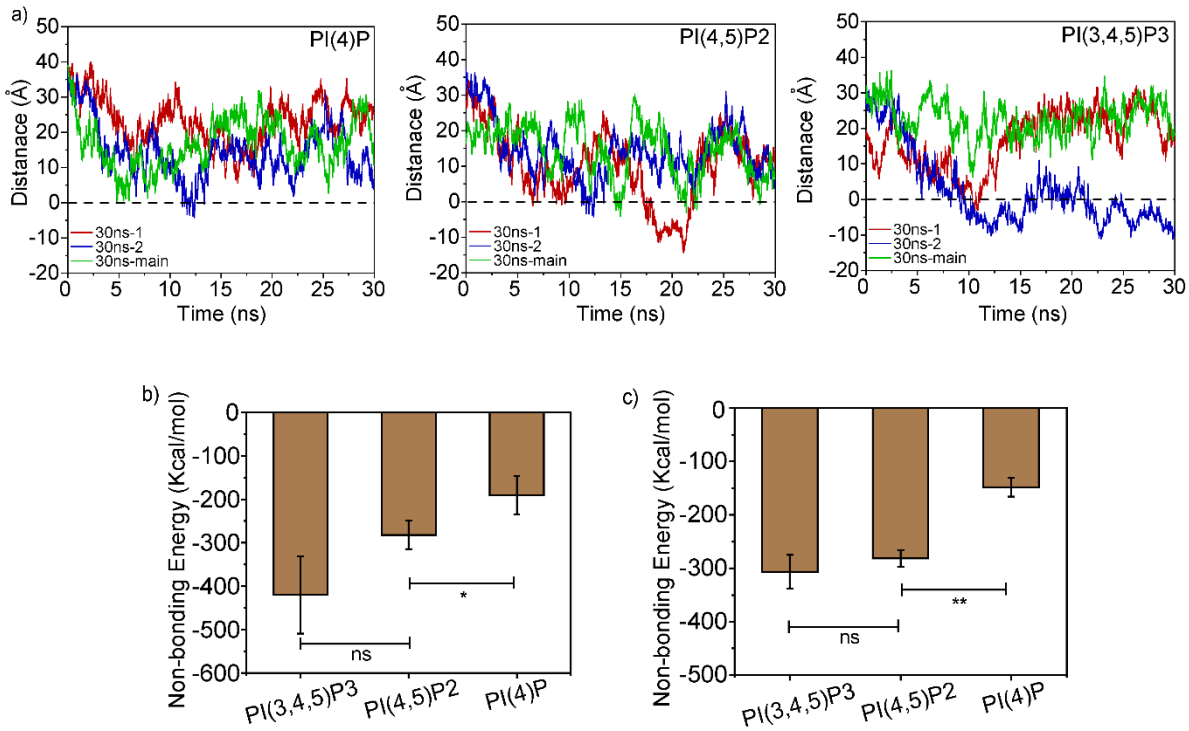

Extended Data Fig. 4| (a) Distributions of the distance between the N-terminus amine group of Gel-20aa and the membrane surface along the z-axis upon binding to PI(4)P, (PI(4,5)P2, and PI(3,4,5)P3 headgroups, respectively. All calculations were done on two independent 30 ns simulations and first 30 ns taken from original 200 ns simulations for Gel-20aa-phosphoinositide-membrane systems. (b) Bar plot representing the average non-bonding energies for phosphoinositide headgroups and Gel-20aa, during 30ns simulations. (c) Bar plot representing the average non-bonding energies for phosphoinositide headgroups and Gel-12aa, during 30ns simulations. Error bars represent SEM. Statistical

analyses were done on 3 independent sets of simulations using an unpaired, two-tailed student's t-test, $*p < 0.05$; $**p < 0.01$.

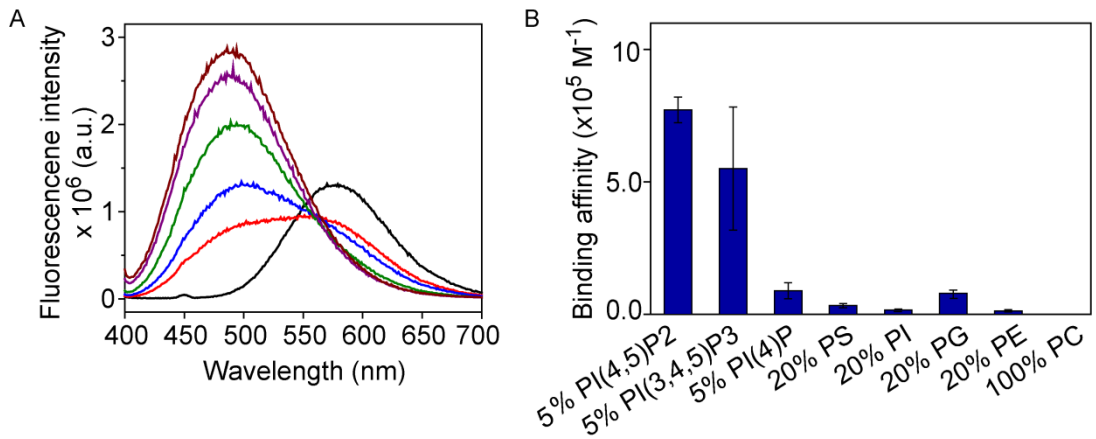

Extended Data Fig. 5| (a) Fluorescence response of **MFR-20aa** (1 µM) depicting a blue shift in emission maxima with increasing concentrations (0, 3, 5, 24, 90, and 113 µM) of 5% PI(4,5)P2-PC SUVs, λ_{ex} 390 nm. (b) Bar plot comparing the association constants (K_a) of **MFR-20aa** toward various PLs, derived from fluorescence titrations. Error bars represent SEM, *N*=3.

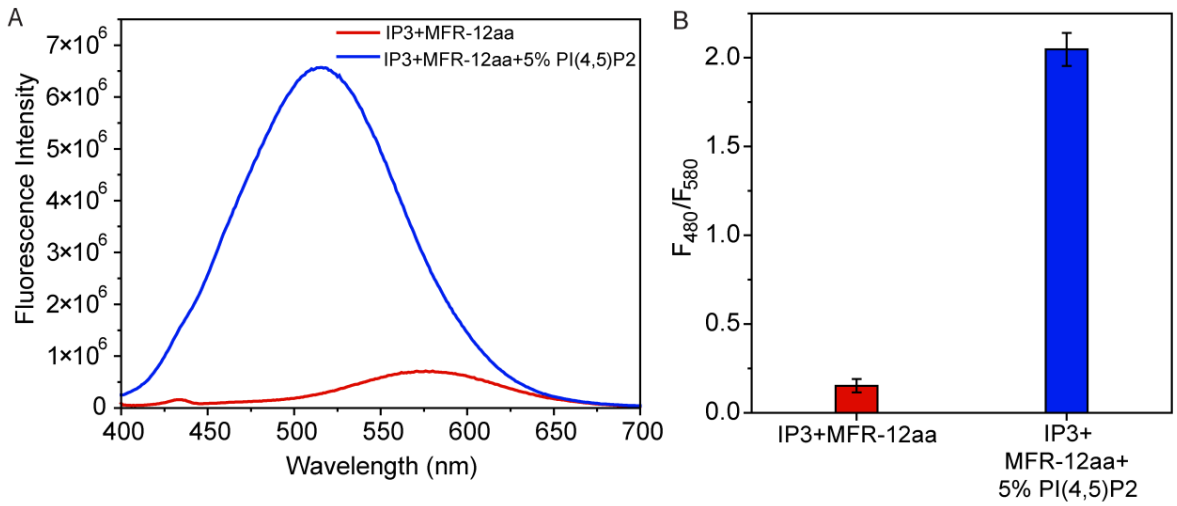

Extended Data Fig. 6| (A) Emission spectra of **MFR-12aa** in presence of IP3 (35 µM, red) and in presence of 5% PI(4,5)P2 (70 µM of total PL) +IP3 (35 µM, blue), λ_{ex} 390 nm. (B) Ratiometric response (F_{480}/F_{580}) of **MFR-12aa** toward IP3 (red) and PI(4,5)P2(70 µM of total PL)+IP3 (35 µM, blue).

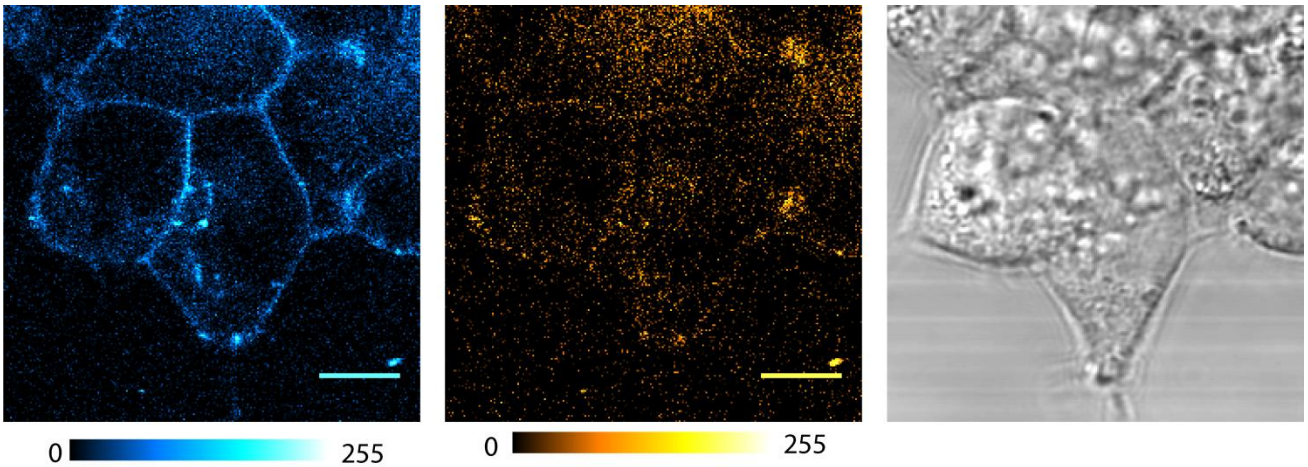

Extended Data Fig. 7| Representative confocal single z-plane images of living HEK293T cells incubated with **MFR-12aa** (5 µM) for 15 min at room temperature. Scale bars, 10 µm. Fluorescence emission: blue channel (λ_{em}: 480−520 nm); orange channel (λ_{em}: 580−620 nm), λ_{ex} 780 nm.

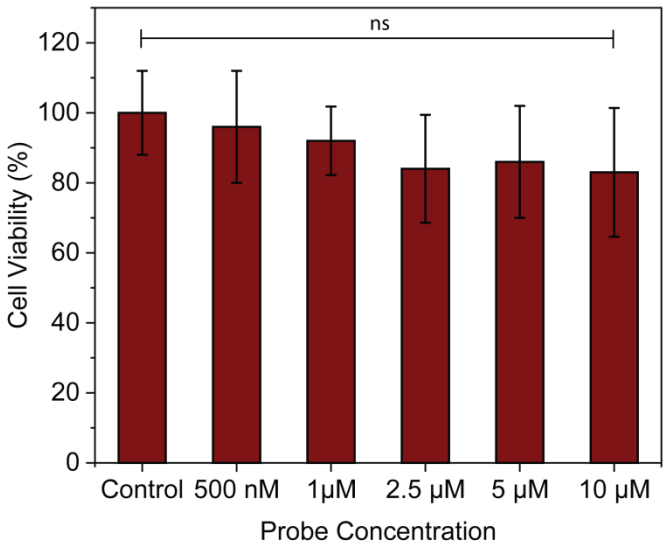

Extended Data Fig. 8| Percentage cell viability in the presence of **MFR-12aa** at different concentrations (0, 0.5, 1, 2.5, 5 and 10 µM) in HEK293T cells after 30 min of incubation at 37 °C in DMEM with no phenol red and serum. Percentage viability was determined by recording absorbance at 570 nm of formazan using MTT assay. Data has been expressed as the mean ± SEM of three independent experiments performed in triplicates, *n*=9, *N*=3.

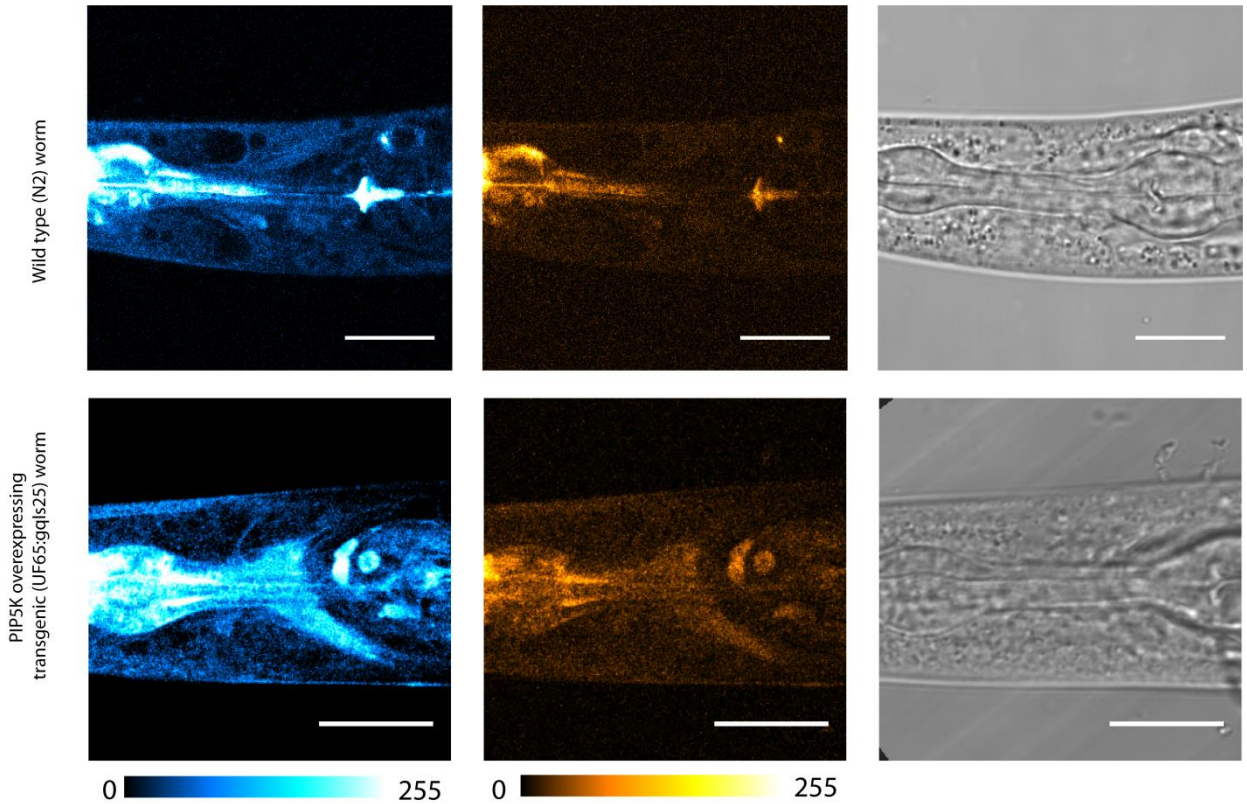

Extended Data Fig. 9| Representative single z-plane images of live *C. elegans,* wild type *N2* (above) and transgenic *gqls25* (below). **MFR-12aa** (10 µM) was excited with 780 nm two-photon laser. Fluorescence emission: blue channel (λ_{em}: 480−520 nm); orange channel (λ_{em}: 580−620 nm).

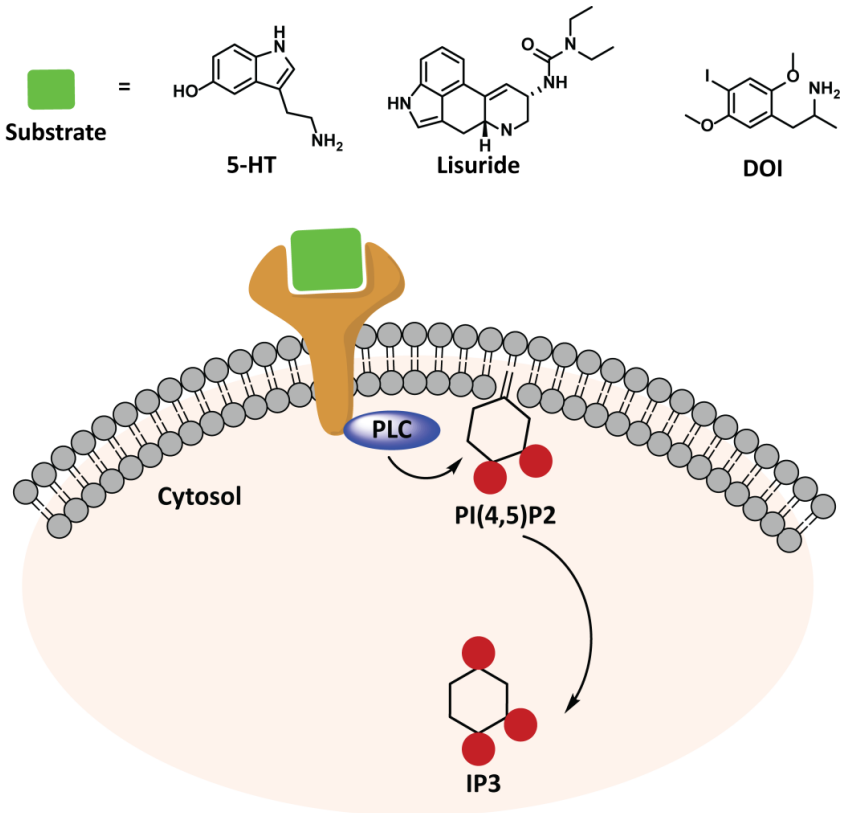

Extended Data Fig. 10| Scheme depicting ligand mediated PI(4,5)P2 dynamics in serotonergic receptor system. Serotonin (5-HT), hallucinogenic (DOI), and non-hallucinogenic (Lisuride) ligands bind to 5-HT_{2A} receptor leading to activation of PLC which cleaves off the PI(4,5)P2 headgroup into IP3 (in cytosol) and DAG (in membrane). Probe binding to PI(4,5)P2 headgroup elicits a response in the membrane which diminishes upon cleavage of PI(4,5)P2 headgroup to IP3. Reversible nature of the probe aids in detection of both depletion and regeneration of PI(4,5)P2 in cellular membranes.

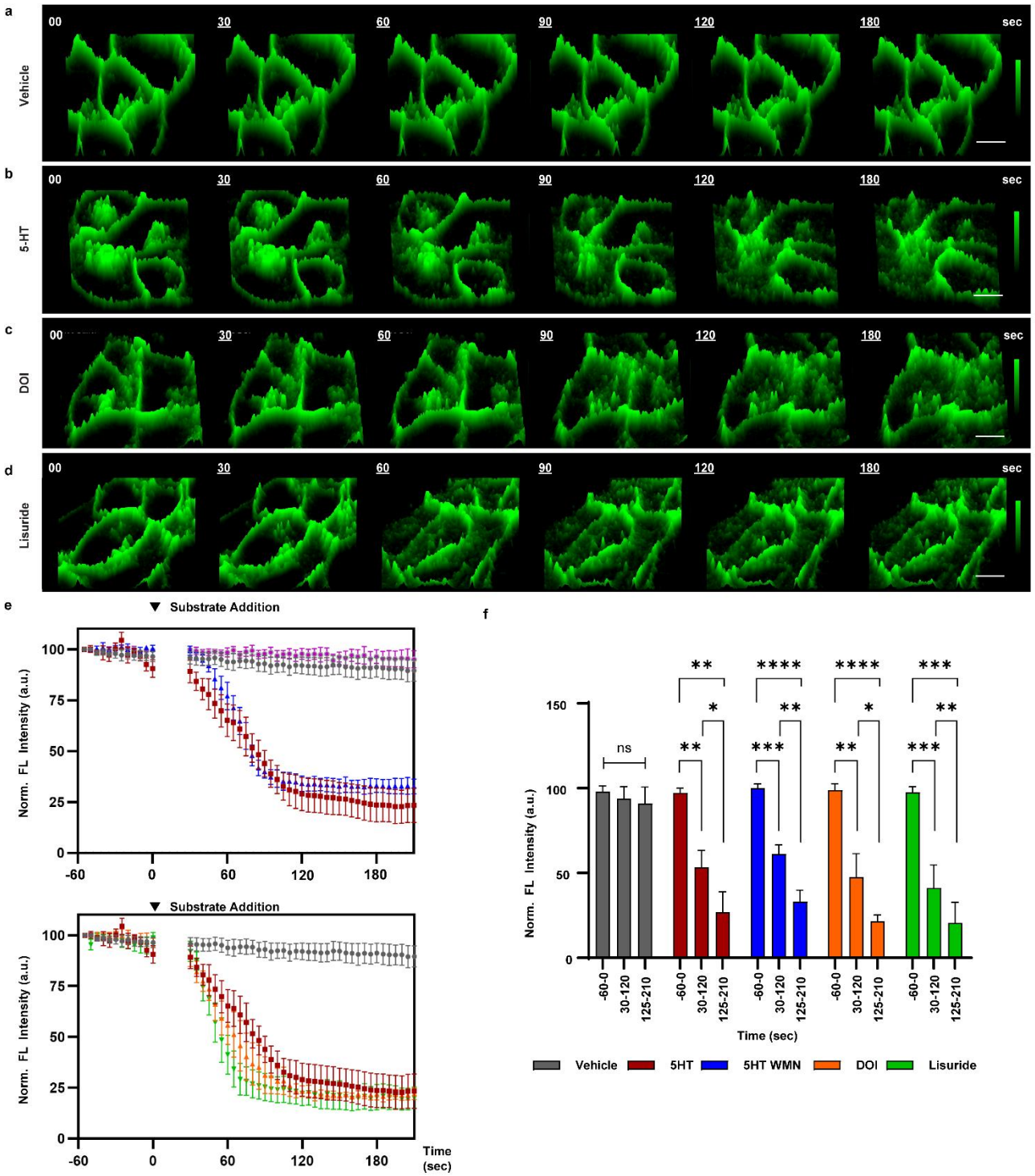
a
Vehicle
b
5-HT
c
DOI
d
Lisuride
00
30
60
90
120
180
sec
e
Substrate Addition
Norm. FL Intensity (a.u.)
Time (sec)
f
Norm. FL Intensity (a.u.)
Time (sec)
ns
-60-0
30-120
125-210
Vehicle
5HT
5HT WMN
DOI
Lisuride

Extended Data Fig. 11 | Visualizing ligand-mediated GFP-tagged 5-HT_{2A} receptor dynamics in live 5-HT_{2A} over-expressing HEK293 cells using confocal time-lapse imaging in the absence of the **MFR-12aa** probe; confocal microscopy λ_{ex} 488 nm, λ_{em} 500-560 nm, scale bar 10 µm. Time trace for a single z-slice, 3D intensity scale representation (0-255) during (a) vehicle and ligand stimulation of (b) 5-HT (10 µM), (c) DOI (10 µM) and (d) Lisuride (10 µM). Data was acquired for unstimulated cells (1 min), ligand stimulation (3 min). Time points during ligand stimulation are underlined. Depicted data is representative of four independent experiments. (e) Time trace of GFP fluorescence intensities depicting differential rates of ligand-dependent 5-HT_{2A} receptor internalization upon stimulation with: 5-HT; 5-HT and WMN; DOI and; Lisuride; compared to vehicle (0.01% DMSO). Percentage intensities were calculated as the ratio of membrane GFP intensity to cytoplasmic GFP intensity, normalized to the initial intensity ratio. (f) Time-dependent intensity analysis bar plots showing the differential internalization rates in the presence and absence of 5-HT, 5-HT and WMN, DOI, and Llisuride (10 µM each, respectively). Error bars represent SEM, *N*=3 (total no. of cells = 30-50 cells); * p = 0.02, ** p = 0.01, *** p = 0.001, **** p = 0.0001 using Student's t test.

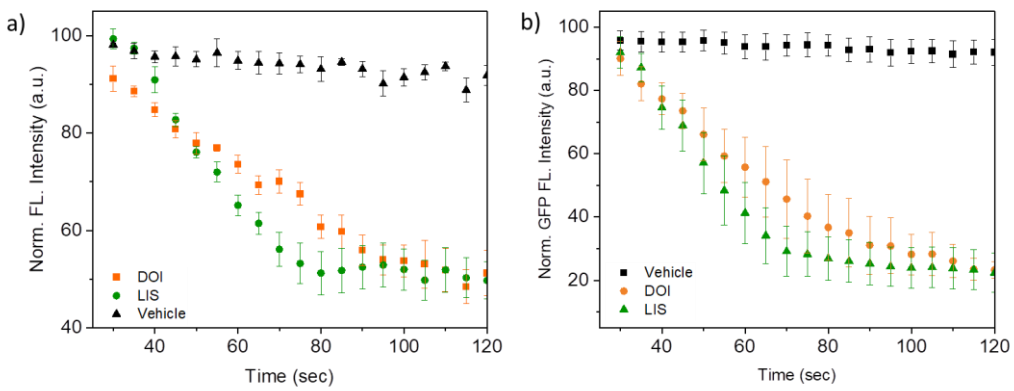

Extended Data Fig. 12 | Zoomed-in representation of 25−120 s time scale to show (a) PI(4,5)P2 depletion tracked by **MFR-12aa** (Fig. 3g) , and (b) GFP tagged 5-HT_{2A} receptor internalization upon agonist (DOI and Lisuride) addition (Extended Data Fig. 11e). Data represented as the mean ± SEM (*N*=3).

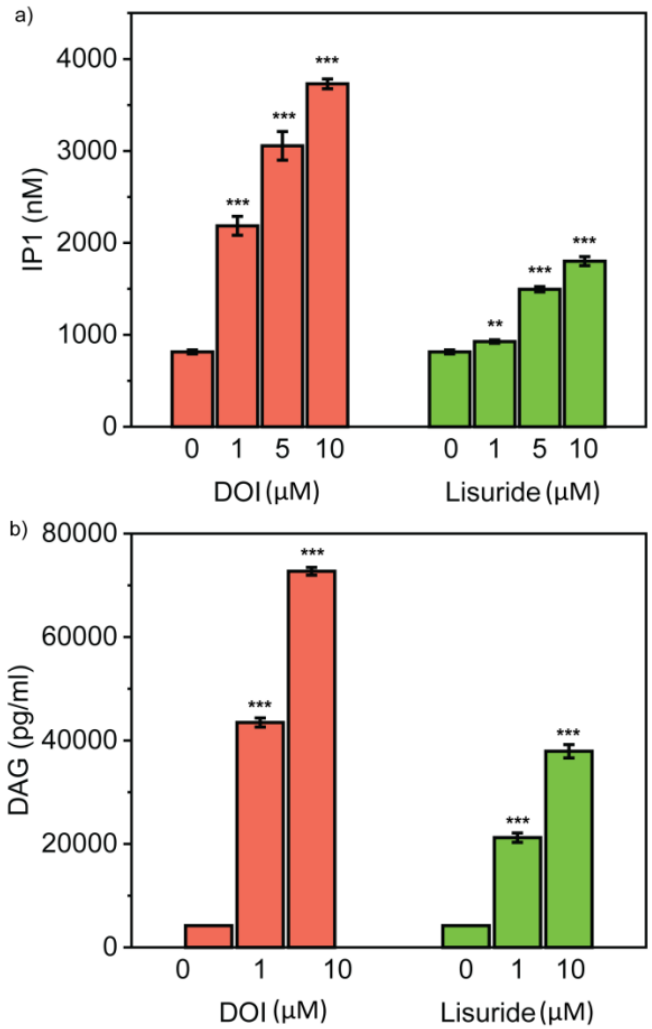

Extended Data Fig. 13| IP1 and DAG assay upon DOI and Lisuride stimulation: HEK293 cells stably expressing human 5-HT_{2A} receptor were either stimulated with increasing doses of DOI (hallucinogen) or Lisuride (non-hallucinogen), followed by measurement of intracellular (a) IP1 (nM) and (b) DAG (pg/mL) production using commercially available ELISA kits. Lisuride induced IP1 and DAG production was significantly lower at all the doses tested. Data has been expressed as the

mean ± SEM of three independent experiments performed in duplicates. The significance of the differences was evaluated by one-way ANOVA followed by Tukey's post hoc test of the Software 'GraphPad Prism 5.0' (GraphPad Software, Inc., San Diego, CA, USA). The values of *p<0.05 with respect to basal values were considered to be statistically significant.

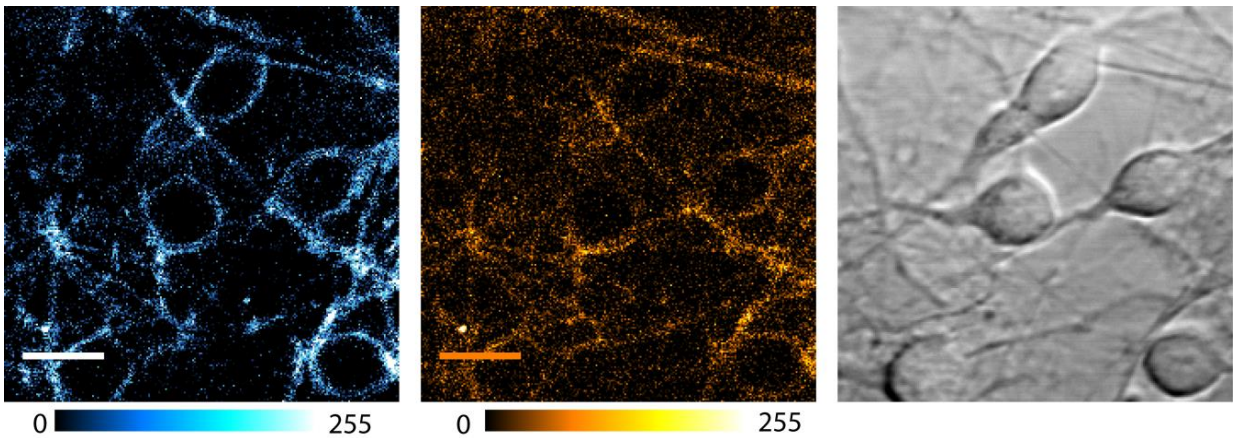

Extended Data Fig. 14| Representative confocal single z-plane images of cortical neurons incubated with **MFR-12aa** sensor (1 µM, 5 min). **MFR-12aa** was excited with 780 nm 2-photon laser. Fluorescence emission: blue channel (λ_{em}: 480−520 nm); orange channel (λ_{em}: 580−620 nm).

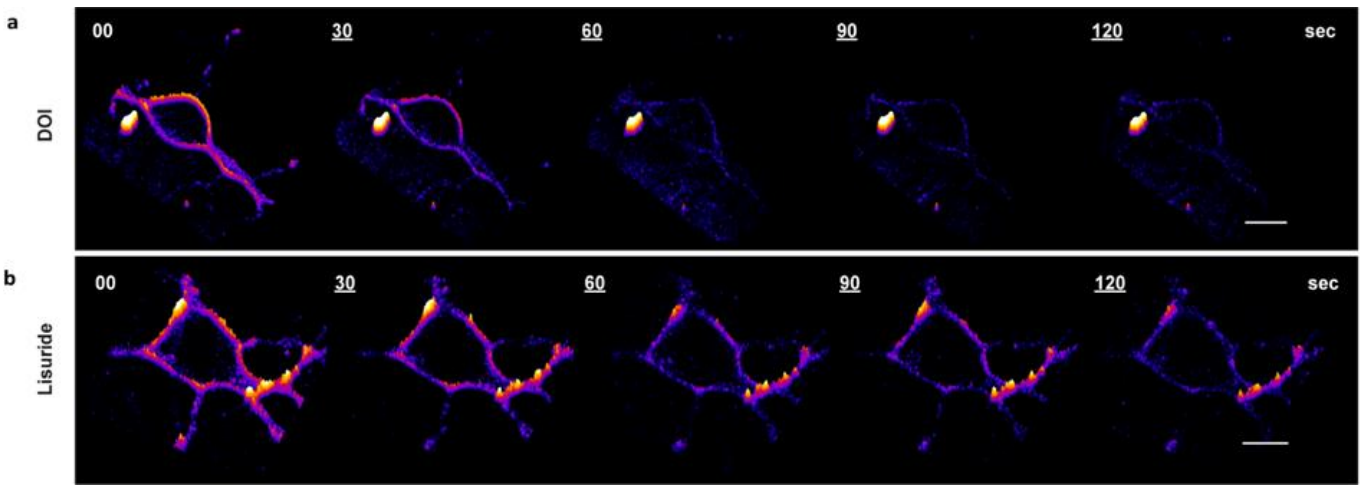

Extended Data Fig. 15| Zoomed-in time frames (Fig. 4c,d) of confocal time-lapse imaging of rat primary cortical neurons incubated with **MFR-12aa** (1 µM), imaged at λ_{ex} 780 nm, λ_{em} 480-520 nm (blue channel), scale bar 10 µm. 3D intensity time traces for a single z-slice during ligand stimulation with (a) DOI (10 µM) and (b) Lisuride (10 µM).

Simulations	Length	Bilayer composition
PI(4,5)P2-Gel-20aa	200 ns*1, 30 ns*2	POPC: PI(4,5)P2
PI(4)P-Gel-20aa	200 ns*1, 30 ns*2	POPC: PI(4)P
PI(3,4,5)P3-Gel-20aa	200 ns*1, 30 ns*2	POPC: PI(3,4,5)P3
PI(4,5)P2-Gel-12aa	30 ns*3	POPC: PI(4,5)P2
PI(4)P- Gel-12aa	30 ns*3	POPC: PI(4)P
PI(3,4,5)P3- Gel-12aa	30 ns*3	POPC: PI(3,4,5)P3

Extended Data Table. 1| Summary of MD simulations done for designing the probes.

Simulations	Extent of N-terminus dipping (Å)	Average binding energy (Kcal/mol)
PI(4,5)P2- Gel-20aa	-14.4	-282.2±32.9
PI(4)P- Gel-20aa	-4.2	-190.7±44.2
PI(3,4,5)P3- Gel-20aa	-11.2	-420.0±89.5
PI(4,5)P2- Gel-12aa	-19.6	-281.4±15.8
PI(4)P- Gel-12aa	-6.2	-147±17.5
PI(3,4,5)P3- Gel-12aa	-17.0	-306.7±31.7

Calculations are done on two independent 30 ns and first 30 ns of the 200 ns run for Gel-20aa-phosphoinositide membrane systems and three independent 30 ns runs of Gel-12aa-phosphoinositide membrane systems.

Extended Data Table. 2| Extent of maximum N-terminal dipping and average binding energy for each simulated system during 30 ns simulations.

Acknowledgments

We acknowledge the kind gift of the human and rat 5-HT2AR-EGFP fusion receptor expressing HEK293 cell lines from Dr. Mitradas Panicker, National Centre for Biological Sciences, Bangalore, India. The authors thank

the cell culture facility, confocal facility, and MALDI facility at the Department of Chemical Sciences, TIFR. A.D. acknowledges support from the Department of Atomic Energy, Government of India, under Project Identification No. RTI4003. A.S.K acknowledges support from Agence Nationale de la Recherche (ANR) AmpliSens ANR-21-CE42-0019-01.

Reference

1 Harayama, T. & Riezman, H. Understanding the diversity of membrane lipid composition. *Nature Reviews Molecular Cell Biology* **19**, 281-296, doi:10.1038/nrm.2017.138 (2018).

2 Yen, H.-Y. *et al.* PtdIns(4,5)P2 stabilizes active states of GPCRs and enhances selectivity of G-protein coupling. *Nature* **559**, 423-427, doi:10.1038/s41586-018-0325-6 (2018).

3 Sarkar, P. & Chattopadhyay, A. Interplay of Cholesterol and Actin in Neurotransmitter GPCR Signaling: Insights from Chronic Cholesterol Depletion Using Statin. *ACS Chemical Neuroscience* **14**, 3855-3868, doi:10.1021/acschemneuro.3c00472 (2023).

4 Posor, Y., Jang, W. & Haucke, V. Phosphoinositides as membrane organizers. *Nature Reviews Molecular Cell Biology* **23**, 797-816, doi:10.1038/s41580-022-00490-x (2022).

5 Di Paolo, G. & De Camilli, P. Phosphoinositides in cell regulation and membrane dynamics. *Nature* **443**, 651-657, doi:10.1038/nature05185 (2006).

6 Balla, T. Phosphoinositides: tiny lipids with giant impact on cell regulation. *Physiological reviews* **93**, 1019-1137, doi:10.1152/physrev.00028.2012 (2013).

7 López-Giménez, J. F. & González-Maeso, J. Hallucinogens and Serotonin 5-HT(2A) Receptor-Mediated Signaling Pathways. *Current topics in behavioral neurosciences* **36**, 45-73, doi:10.1007/7854_2017_478 (2018).

8 Schultz, C. Challenges in studying phospholipid signaling. *Nature Chemical Biology* **6**, 473-475, doi:10.1038/nchembio.389 (2010).

9 Yang, Y., Lee, M. & Fairn, G. D. J. J. o. B. C. Phospholipid subcellular localization and dynamics. **293**, 6230-6240 (2018).

10 Jensen, J. B. *et al.* Biophysical physiology of phosphoinositide rapid dynamics and regulation in living cells. *The Journal of general physiology* **154**, doi:10.1085/jgp.202113074 (2022).

11 Kundu, R., Chandra, A. & Datta, A. Fluorescent Chemical Tools for Tracking Anionic Phospholipids. *Israel Journal of Chemistry* **61**, 199-216, doi:https://doi.org/10.1002/ijch.202100003 (2021).

12 Lemmon, M. A. Membrane recognition by phospholipid-binding domains. *Nature Reviews Molecular Cell Biology* **9**, 99-111, doi:10.1038/nrm2328 (2008).

13 Cao, E., Cordero-Morales, J. F., Liu, B., Qin, F. & Julius, D. TRPV1 channels are intrinsically heat sensitive and negatively regulated by phosphoinositide lipids. *Neuron* **77**, 667-679, doi:10.1016/j.neuron.2012.12.016 (2013).

14 Várnai, P. & Balla, T. Live cell imaging of phosphoinositide dynamics with fluorescent protein domains. *Biochimica et biophysica acta* **1761**, 957-967, doi:10.1016/j.bbalip.2006.03.019 (2006).

15 Yip, S.-C. *et al.* Quantification of PtdIns(3,4,5)P3 dynamics in EGF-stimulated carcinoma cells: a comparison of PH-domain-mediated methods with immunological methods. *Biochemical Journal* **411**, 441-448, doi:10.1042/BJ20071179 %J Biochemical Journal (2008).
16 Xu , C., Watras , J. & Loew , L. M. Kinetic analysis of receptor-activated phosphoinositide turnover. *Journal of Cell Biology* **161**, 779-791, doi:10.1083/jcb.200301070 %J Journal of Cell Biology (2003).
17 Tuominen, E. K. J. *et al.* Fluorescent phosphoinositide derivatives reveal specific binding of gelsolin and other actin regulatory proteins to mixed lipid bilayers. *European Journal of Biochemistry* **263**, 85-92, doi:https://doi.org/10.1046/j.1432-1327.1999.00464.x (1999).
18 Kleusch, C., Hersch, N., Hoffmann, B., Merkel, R. & Csiszár, A. Fluorescent Lipids: Functional Parts of Fusogenic Liposomes and Tools for Cell Membrane Labeling and Visualization. *Molecules* **17**, 1055-1073 (2012).
19 Yoshioka, D. *et al.* Single-molecule imaging of PI(4,5)P2 and PTEN in vitro reveals a positive feedback mechanism for PTEN membrane binding. *Communications Biology* **3**, 92, doi:10.1038/s42003-020-0818-3 (2020).
20 Rhee, S. G., Suh, P.-G., Ryu, S.-H. & Lee, S. Y. Studies of Inositol Phospholipid-Specific Phospholipase C. *Science* **244**, 546-550, doi:10.1126/science.2541501 (1989).
21 Klymchenko, A. S. Solvatochromic and Fluorogenic Dyes as Environment-Sensitive Probes: Design and Biological Applications. *Accounts of Chemical Research* **50**, 366-375, doi:10.1021/acs.accounts.6b00517 (2017).
22 Mondal, S., Rakshit, A., Pal, S. & Datta, A. Cell Permeable Ratiometric Fluorescent Sensors for Imaging Phosphoinositides. *ACS Chemical Biology* **11**, 1834-1843, doi:10.1021/acschembio.6b00067 (2016).
23 Xian, W., Vegners, R., Janmey, P. A. & Braunlin, W. H. Spectroscopic studies of a phosphoinositide-binding peptide from gelsolin: behavior in solutions of mixed solvent and anionic micelles. *Biophysical Journal* **69**, 2695-2702, doi:https://doi.org/10.1016/S0006-3495(95)80140-2 (1995).
24 Nasuhoglu, C. *et al.* Nonradioactive analysis of phosphatidylinositides and other anionic phospholipids by anion-exchange high-performance liquid chromatography with suppressed conductivity detection. *Analytical biochemistry* **301**, 243-254, doi:10.1006/abio.2001.5489 (2002).
25 Tauer, U. Advantages and Risks of Multiphoton Microscopy in Physiology. **87**, 709-714, doi:https://doi.org/10.1113/eph8702464 (2002).
26 Kucherak, O. A., Didier, P., Mély, Y. & Klymchenko, A. S. Fluorene Analogues of Prodan with Superior Fluorescence Brightness and Solvatochromism. *The Journal of Physical Chemistry Letters* **1**, 616-620, doi:10.1021/jz9003685 (2010).
27 Leventis, P. A. & Grinstein, S. The distribution and function of phosphatidylserine in cellular membranes. *Annual review of biophysics* **39**, 407-427, doi:10.1146/annurev.biophys.093008.131234 (2010).
28 Weinkove, D. *et al.* Overexpression of PPK-1, the Caenorhabditis elegans Type I PIP kinase, inhibits growth cone collapse in the developing nervous system and causes axonal degeneration in adults. *Dev Biol* **313**, 384-397, doi:10.1016/j.ydbio.2007.10.029 (2008).
29 Bhattacharyya, S., Puri, S., Miledi, R. & Panicker, M. M. Internalization and recycling of 5-HT2A receptors activated by serotonin and protein kinase C-mediated mechanisms. *Proceedings of the*

National Academy of Sciences of the United States of America **99**, 14470-14475, doi:10.1073/pnas.212517999 (2002).

30 Calloway, N. *et al.* Stimulated association of STIM1 and Orai1 is regulated by the balance of PtdIns(4,5)P2 between distinct membrane pools. *Journal of Cell Science* **124**, 2602-2610, doi:10.1242/jcs.084178 %J Journal of Cell Science (2011).

31 Xie, L.-H., Takano, M., Kakei, M., Okamura, M. & Noma, A. Wortmannin, an inhibitor of phosphatidylinositol kinases, blocks the MgATP-dependent recovery of Kir6.2/SUR2A channels. **514**, 655-665, doi:https://doi.org/10.1111/j.1469-7793.1999.655ad.x (1999).

32 González-Maeso, J. *et al.* Hallucinogens Recruit Specific Cortical 5-HT2A Receptor-Mediated Signaling Pathways to Affect Behavior. *Neuron* **53**, 439-452, doi:https://doi.org/10.1016/j.neuron.2007.01.008 (2007).

33 Pieri, L., Keller, H. H., Burkard, W. & Da Prada, M. Effects of lisuride and LSD on cerebral monoamine systems and hallucinosis. *Nature* **272**, 278-280, doi:10.1038/272278a0 (1978).

34 Bhattacharya, A., Sankar, S. & Panicker, M. M. Differences in the C-terminus contribute to variations in trafficking between rat and human 5-HT2A receptor isoforms: identification of a primate-specific tripeptide ASK motif that confers GRK-2 and β arrestin-2 interactions. *Journal of Neurochemistry* **112**, 723-732, doi:https://doi.org/10.1111/j.1471-4159.2009.06493.x (2010).

35 Willars, G. B., Nahorski, S. R. & Challiss, R. A. Differential regulation of muscarinic acetylcholine receptor-sensitive polyphosphoinositide pools and consequences for signaling in human neuroblastoma cells. *The Journal of biological chemistry* **273**, 5037-5046, doi:10.1074/jbc.273.9.5037 (1998).

36 Pazos, A., Probst, A. & Palacios, J. M. Serotonin receptors in the human brain—IV. Autoradiographic mapping of serotonin-2 receptors. *Neuroscience* **21**, 123-139, doi:https://doi.org/10.1016/0306-4522(87)90327-7 (1987).

37 Micheva, K. D., Holz, R. W. & Smith, S. J. Regulation of presynaptic phosphatidylinositol 4,5-biphosphate by neuronal activity. *Journal of Cell Biology* **154**, 355-368, doi:10.1083/jcb.200102098 (2001).

38 Cornea-Hébert, V. *et al.* Similar ultrastructural distribution of the 5-HT2A serotonin receptor and microtubule-associated protein MAP1A in cortical dendrites of adult rat. *Neuroscience* **113**, 23-35, doi:https://doi.org/10.1016/S0306-4522(02)00146-X (2002).

39 Senju, Y. *et al.* Mechanistic principles underlying regulation of the actin cytoskeleton by phosphoinositides. *Proceedings of the National Academy of Sciences of the United States of America* **114**, E8977-e8986, doi:10.1073/pnas.1705032114 (2017).